

Scale-dependent influence of permafrost on riverbank erosion rates.

Joel C. Rowland¹, Jonathan P. Schwenk¹, Eitan Shelef², Jordan Muss³, Daniel Ahrens⁴, Sophie Stauffer¹, Anastasia Pilliouras⁵, Benjamin Crosby⁶, Austin Chadwick⁷, Madison Douglas⁷, Preston C. Kemeny⁷, Michael P. Lamb⁷, Gen Li⁸, and Lawrence Vulis⁹

¹ Earth and Environmental Sciences Division, Los Alamos National Laboratory, Los Alamos, New Mexico, USA

² Department of Geology and Environmental Sciences University of Pittsburgh, Pittsburgh, PA, USA

³ General Atomics Commonwealth Computer Research, Inc., Charlottesville, VA, USA

⁴ Stanford Law School, Stanford, CA, USA

⁵ Department of Geosciences, Pennsylvania State University, University Park, PA, USA

⁶ Department of Geosciences, Idaho State University, Pocatello, ID, USA

⁷ Division of Geological and Planetary Sciences, California Institute of Technology, Pasadena, California, USA

⁸ Department of Earth Science, University of California Santa Barbara, Santa Barbara, CA, USA

⁹ Department of Civil and Environmental Engineering, University of California Irvine

Key Points:

- Permafrost systematically reduces riverbank erosion rates in Arctic and subarctic rivers by 6 times compared to lower latitude rivers
- The influence of permafrost on small rivers is limited but increases with river size
- Permafrost thaw due to climate change will likely increase erosion rates on large rivers and have a limited impact on small rivers

Plain Language Summary

The rate rivers erode their banks controls the pace of migration and the impacts on neighboring communities and ecosystems. Across the Arctic, rivers erode through floodplains frozen continuously for more than two years (permafrost). Before frozen sediments can be eroded by flowing water they must be thawed. Using aerial photographs, satellite imagery, and direct field observations we found that permafrost slows the rate rivers erode their banks relative to rivers without permafrost. The effect of permafrost, however, varies with the size of the river and the erosion rates of large rivers are disproportionately slowed by permafrost. As a result, permafrost thaw due to climate change will likely increase erosion rates on large rivers and have limited impact on small rivers, but very little data is available for small rivers in the Arctic.

Abstract

Whether the presence of permafrost systematically alters the rate of riverbank erosion is a fundamental geomorphic question with significant importance to infrastructure, water quality, and biogeochemistry of high latitude watersheds. For over four decades this question has remained unanswered due to a lack of data. Using remotely sensed imagery, we addressed this knowledge gap by quantifying riverbank erosion rates across the Arctic and subarctic. To compare these rates to non-permafrost rivers we assembled a global dataset of published riverbank erosion rates. We found that erosion rates in rivers influenced by permafrost are on average six times lower than non-permafrost systems; erosion rate differences increase up to 40

times for the largest rivers. To test alternative hypotheses for the observed erosion rate difference, we examined differences in total water yield and erosional efficiency between these rivers and non-permafrost rivers. Neither of these factors nor differences in river sediment loads provided compelling alternative explanations, leading us to conclude that permafrost limits riverbank erosion rates. This conclusion was supported by field investigations of rates and patterns of erosion along three rivers flowing through discontinuous permafrost in Alaska. Our results show that permafrost limits maximum bank erosion rates on rivers with stream powers greater than 900 W/m^{-1} . On smaller rivers, however, hydrology rather than thaw rate may be dominant control on bank erosion. Our findings suggest that Arctic warming and hydrological changes should increase bank erosion rates on large rivers but may reduce rates on rivers with drainage areas less than a few thousand km^2 .

1 Introduction

At water-level, the erosion of frozen bank materials by rivers leaves distinctive morphological features indicative of the presence of permafrost (ground that remains below 0°C for two or more years). These features include thermal-erosion niching (bank undercutting), massive cantilever failures in non-cohesive sediments, and exposed ground ice (Figure 1). From above and at larger spatial scales, however, no clear morphological signature of permafrost has been documented in river planform. Due to this lack of a planform signature of permafrost on rivers an examination of riverbank erosion rates is required to answer the fundamental question: Does the presence of permafrost have an observable effect on rivers dynamics? For over 40 years studies of individual rivers that flow through floodplains with permafrost have observed possible, though often contradictory, influences of frozen sediment and ice on the rates of riverbank erosion (Chassiot et al., 2020; Debol'skaya & Ivanov, 2020; Gatto, 1984; Gautier et al., 2021; Lawson, 1983; Scott, 1978; Tananaev, 2016). Due to these contradictory results and a dearth of data, a clear answer to whether rivers erode floodplains with permafrost at different rates than other rivers has remained elusive.

The potential influence of permafrost on the rates of riverbank erosion has great relevance to communities in the Arctic. Locally, Arctic rivers are major transportation arteries and provide significant food resources to local populations (Brinkman et al., 2016; Cold et al., 2020; Hovelsrud et al., 2011; Instanes et al., 2016; Payne et al., 2018). Bank erosion in these systems threatens to undermine infrastructure (University of Alaska Fairbanks Institute of Northern Engineering et al., 2019) and cause village relocations, especially in Alaska (Figures S2 and #), where 43% of villages are located less than one kilometer from riverbanks (Supporting Text S1 and Figure S1).

Arctic rivers carry substantial chemical fluxes (Drake et al., 2018; Schuur et al., 2015; Tank et al., 2012), which may change in response to the warming climate and feedback on atmospheric chemistry. Currently, Arctic rivers account for approximately 8% of the total organic carbon (TOC) flux to global oceans (Rachold et al., 2004) and export 34 Tg of dissolved organic carbon (DOC) (Holmes et al., 2012) and 5.8 Tg of particulate organic carbon (POC) (McClelland et al., 2016) each year.

Studies of Arctic river chemistry suggest that bank erosion contributes a significant fraction of riverine POC (Striegl et al., 2007) and that bank-derived carbon influences the age and composition of carbon in both rivers and the Arctic ocean basin (Gustafsson et al., 2011; Mann et al., 2015; Wild et al., 2019). Recent modeling studies suggest that riverine fluxes of

carbon and nutrients play a significant role in the net primary productivity of the Arctic Ocean (Terhaar et al., 2021).

River migration and floodplain erosion strongly influences carbon cycling in watersheds (Torres et al., 2017). However, studies in Alaska conflict regarding the extent to which river migration influences floodplain carbon storage. A Yukon River study of the variability of floodplain carbon suggested river migration was an important control on floodplain carbon storage (Lininger et al., 2018, 2019), while a study of the Koyukuk River, AK showed little difference in carbon quantity or characteristics between eroding banks and newly deposited point bars (Douglas et al., 2022).



Figure 1: Images of riverbanks eroding permafrost. a) Thermal-erosion niche undercutting a bank composed of frozen sand along the Yukon River, in central AK. b) Massive failure blocks resulting from thermal erosion undercutting of banks along the Yukon River, AK (66.33 N, 147.60 W). The top of the bank is approximately 4 m above the waterline. c) Exposed ice wedge and associated bank erosion in the banks of the Yukon River, AK. d) Thermal denudation and collapse of an ice-rich bank along the Koyukuk River (65.780 N, 156.437 W). Shovel

handle in center of photo for scale. e) Sediments piled up on riverbank due to river ice erosion and sediment transport on the Yukon River, AK. f) Riverbank along the Selawik River in July 2012 showing loose thawed gravels and tundra blocks from spring bank erosion protecting the bank face (66.48 N, 157.71 W). Location of images shown on Figure 3.

2 Background

2.1 State of knowledge regarding permafrost influence on riverbank erosion

The presence of permafrost alters the hydrological, vegetation, and geomechanical characteristics of riverbanks in ways that may influence the rates bank erosion. Hydrologically, permafrost acts as a largely impermeable layer restricting water infiltration and liquid saturation of soils to a seasonally thawed shallow surface layer (French, 2007; Hinzman et al., 2005; Woo & Winter, 1993). This impermeability also prevents the periodic saturation and draining of riverbank faces that can lead to pore pressure-driven bank collapse commonly observed in seasonally unfrozen banks (Darby & Thorne, 1996; Rinaldi & Casagli, 1999; Tananaev & Lotsari, 2022; Zhao et al., 2022). The role of vegetation in stabilizing riverbanks (Simon & Collison, 2002) may be limited by permafrost restricting rooting depth to shallow seasonally thawed surface layers (Blume-Werry et al., 2019; Jackson et al., 1996). Geomechanically, frozen pore waters provide additional strength to the soil matrix relative to the same material in an unfrozen state (Cooper & Hollingshead, 1973; Lawson, 1983; Shur et al., 2002; Tsytovich, 1975; Williams & Smith, 1991). This additional strength and cementation of grains by ice requires that the frozen sediments thaw before being physically eroded by water (Are, 1983; Randriamazaoro et al., 2007; Shur et al., 2002; Walker et al., 1987). The additional mechanical strength provided by ice also leads to dramatic undercutting of banks creating distinctive thermal erosion niches (Walker et al., 1987) and large cantilever failure blocks (Figure 1b).

The geomechanical strength imparted to bank materials is lost upon thawing and riverbanks erode by a combination of thaw and physical transport of thawed material (thermal abrasion) (Are, 1983; Cooper & Hollingshead, 1973; Costard et al., 2003; Lawson, 1983; Leffingwell, 1919; Miles, 1976; Scott, 1978; Walker et al., 1987; Walker & Arnborg, 1963; Zhang et al., 2022). Therefore, the rate of bank erosion may be set by the combined effects of thermal and physical processes. The thaw rates of frozen sediments decrease with increasing ice content (Randriamazaoro et al., 2007; Shur et al., 2002; J. R. Williams, 1952a), and increase with larger grain sizes (Scott, 1978; Shur et al., 2002), river discharge, and water temperature (Shur et al., 2002), with a greater sensitivity to temperature than discharge (Costard et al., 2003; Dupeyrat et al., 2011; Randriamazaoro et al., 2007). Though thaw rates may slow with increasing ice content, the presence of excess ice may augment the net erosion rates of some deposits relative to similar unfrozen, ice-free materials (Gatto, 1984; Shur et al., 2002) due to a loss of cohesion upon thawing (Dupeyrat et al., 2011) and/or because the volume of sediment to be eroded decreases with increasing ice content (Are, 1983; Lawson, 1983). Melting ice may also lead to saturation in fine grained, poorly-draining sediments, triggering flow and collapse of thawing sediments, commonly referred to as thermal denudation (Kanevskiy et al., 2016) (Figure 1D). If flowing water and/or slopewash on the bank remove thawed material the subaerial portion of the bank remains exposed to thawing and continues to retreat independent of fluvial erosion (Kanevskiy et al., 2016; Lawson, 1983; Shur et al., 2021; Stettner et al., 2018).

Whether the effects of permafrost on hydrological, vegetation, and geomechanical properties of riverbanks results in a measurable or systematic influence on riverbank erosion rates has not been resolved to date. Past reviews of studies of riverbank erosion rates in permafrost regions failed to reach a conclusion on the role of permafrost (Lawson, 1983; Scott,

1978). Lawson (1983) and Scott (1978) both concluded that quantifying the role of permafrost was confounded by other possible controls, such as hydrology, climate, and local bank conditions, and hindered by an absence of comprehensive studies of erosion rates in both permafrost and non-permafrost watersheds. More recent studies, continue to cite the lack of long-term and large-scale observations as an ongoing challenge to quantifying the role of permafrost in riverbank erosion (Chassiot et al., 2020; Debol'skaya & Ivanov, 2020; Gautier et al., 2021; Tananaev, 2016).

Studies of individual rivers have reached conflicting conclusions regarding the relative influence of permafrost on riverbank erosion rates. Leffingwell (1919) argued that frozen sediments reduced bank erosion while Cooper and Hollingshead (1973) suggested that rivers with permafrost should have relatively constant erosion rates from year to year. Are (1983), however, argued that permafrost has no observable impact on riverbank erosion rates. In a study of the Tanana River, AK, Gatto (1984) could not find a clear relationship between permafrost occurrence and erosion rates. On the Lena River, island head retreat rates were 50 to 100% lower where permafrost was present until increases in the combined temperature and discharge of the river led to periods of equal or greater (40%) erosion on these islands (Gautier et al., 2021).

The potential for other regional drivers, such as climate and hydrology, to affect riverbank erosion rates highlighted by previous studies still represents an ongoing challenge to isolate the influence of permafrost. Hydrologically, northern rivers exhibit highly seasonal discharge with peak flows associated with snowmelt runoff (nival) occurring over a few weeks in late spring to early summer, and very limited to no flows (for smaller streams) during winter when covered by ice (Holmes, Coe, et al., 2012; Lafrenière & Lamoureux, 2019; Woo et al., 2008). Observations along permafrost-dominated rivers suggest that local hydrology (Costard et al., 2007, 2014) and the seasonality of river discharge can substantially affect local riverbank thaw and erosion rates along individual rivers (Are, 1983; Randriamazaoro et al., 2007; Tananaev, 2016).

Relative to other regions of the earth, many Arctic rivers have low sediment loads (Rachold et al., 2004). Arctic rivers account for 10% of the global river discharge to oceans (Holmes et al., 2012) but only 1% of the global sediment flux (Gordeev, 2006). On rivers outside the Arctic, sediment loading has been suggested to have a strong positive influence on bank erosion rates (Bufe et al., 2016; Constantine et al., 2014; Dietrich et al., 1999; Donovan et al., 2021; Dunne et al., 1981, 2010; Torres et al., 2017; Wickert et al., 2013), although other studies argue that, at least locally, high sediment loads may be the result of high bank erosion rates and not a driver (Dingle et al., 2020).

Ice is also a distinctive characteristic of northern rivers. The annual break up of winter ice on high latitude rivers plays a major role in flooding (Prowse & Beltaos, 2002) and has also been observed to have dramatic local impacts on banks and riparian vegetation (Ettema, 2002; Gautier et al., 2021; Prowse & Culp, 2003; Scrimgeour et al., 1994) (Figure 1E). Regions of widespread surface ice (aufeis) have been attributed to flow diversion and channel widening along Alaskan north slope rivers (Wohl & Scamardo, 2022). At reach- to watershed-scale, however, the effect of ice on bank erosion remains uncertain with studies concluding that ice has minimal influence (Eardley, 1938; Williams, 1952, 1955), to ice protecting banks (Costard et al., 2014; Miles, 1976; Prowse & Culp, 2003), to ice increasing bank erosion (Brown et al., 2020; Chassiot et al., 2020; Prowse & Culp, 2003) while other studies suggest the available data is inconclusive (Ettema, 2002).

2.2 Potential response of high latitude rivers to a changing climate

Recent reviews have synthesized understanding of river and floodplain dynamics and hypothesized how competing and compounding climatic changes may impact the dynamics of rivers with permafrost. Lininger and Wohl (2019) hypothesized that increased river discharges and loss of permafrost would potentially lead to an acceleration of erosion rates; however, they also noted that the possible influx of sediment from rapidly eroding permafrost landscapes could outpace river transport capacities that would in turn drive aggradation of river channels and lead to net bank accretion. Tananaev and Lotsari (2022) concluded that increased water temperatures, flooding, and sediment loads would most likely drive an increase in riverbank erosion, but that floodplain subsidence could decrease erosion rates.

Only a few multi-temporal studies of riverbank erosion rates in the Arctic exist to allow for an examination of how historical hydrological and climate changes have altered bank erosion rates. In a study of erosion along subArctic rivers in central Alaska, (Brown et al., 2020) observed increased erosion rates correlated with a greater cold season discharge and earlier ice break up on the Yukon and Tanana Rivers. In contrast, the Chandalar River showed increased erosion correlated to colder spring temperatures, potentially related to more vigorous ice-driven erosion during the break-up period (Brown et al., 2020). Studies on the Lena River have reported increases and changes in island head erosion rates that were correlated with river temperature increases (Costard et al., 2007; Gautier et al., 2021).

3 Data Collection and Methods

3.1 Global and pan-Arctic analysis

3.1.1 Global compilation of published erosion rates and watershed characteristics

To compare erosion rates measured in watersheds with permafrost to ones without permafrost, we compiled 993 measurements of riverbank erosion from 336 rivers and streams from 169 published English language studies (Figure 2a) (Rowland & Schwenk, 2019). Drainage areas ranged from 0.15 to 3,000,000 km² and spanned rivers with widths of 1 m to 13 km. The dataset included rivers in 17 of the 30 Köppen-Geiger climate zones (Beck et al., 2018). Previously published studies of erosion rates in high latitude rivers comprised 9 % of studies in our global compilation.

Channel width, river drainage area, and sediment load and/or yield were recorded if provided in a published study; otherwise, we assembled these ancillary data from other published studies, global and regional datasets, or measured representative widths from Google Earth images (Rowland & Schwenk, 2019). We used sediment load data from the Land2Sea (L2S) (Peucker-Ehrenbrink, 2009) dataset for many rivers where that information was not available elsewhere. If unique values for width, drainage area, discharge, and slope were not available for individual erosion rates from the same river, we averaged the erosion rates to provide a single value for each set of river characteristics. This averaging reduced the dataset to 585 measurements for lower-latitude rivers and 36 for published studies of high latitude rivers.

We classified published erosion rates into two categories based on the spatial scale over which the measurements were made: local, such as at an individual bend, and reach. We then only used the reach-scale measurements to compare to our new measurements of erosion rates in permafrost systems. Errors were rarely reported in previous published studies, therefore, we

assigned a standard error of the mean erosion rate of 2% based on the average standard error quantified for our high latitude river dataset.

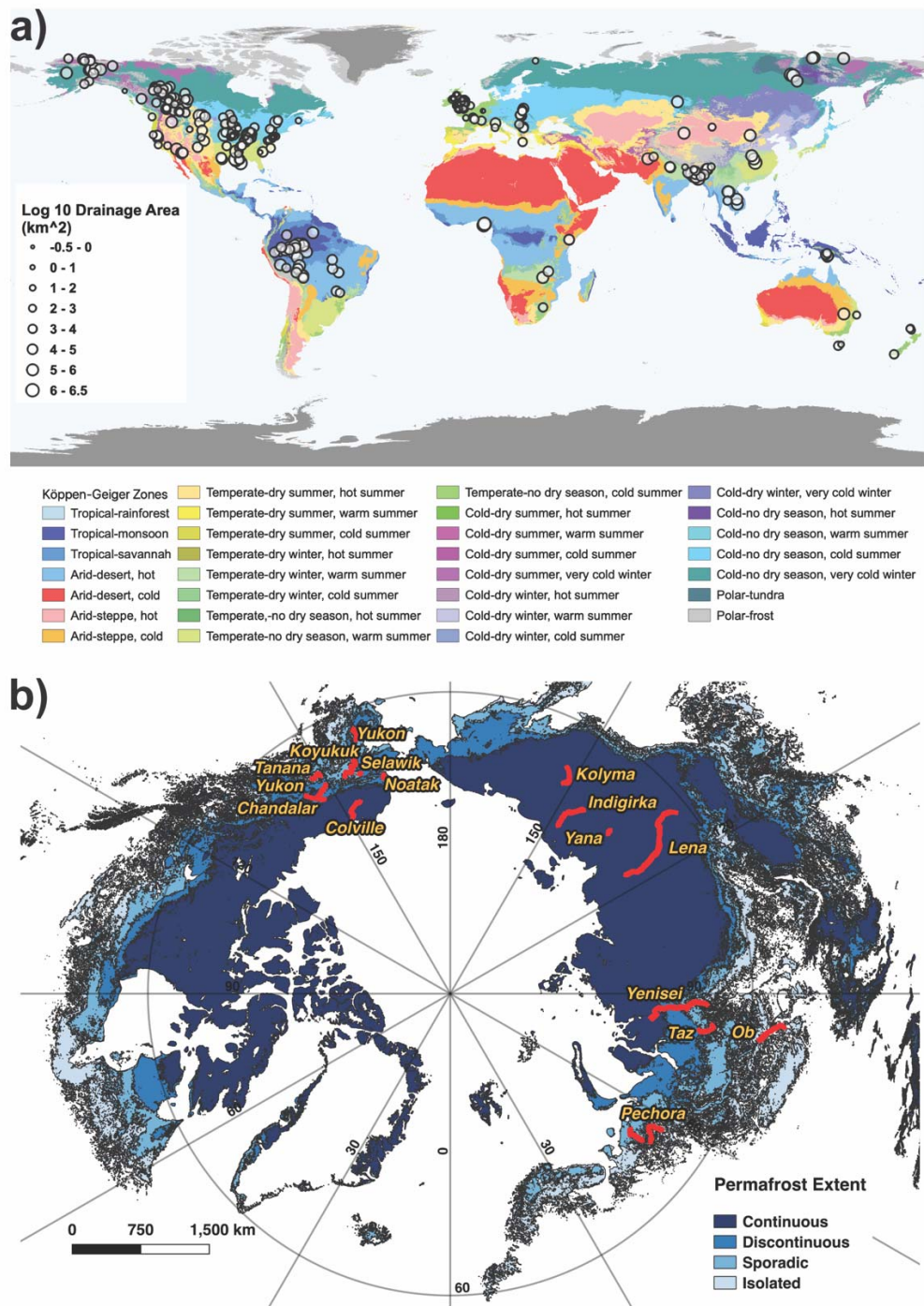


Figure 2: a) Locations of erosion rates compiled from published studies (Rowland & Schwenk, 2019). Circle size is logarithmically (base 10) scaled to the upstream drainage area. The underlying map is colored by the Köppen-Geiger climate zone (Beck et al., 2018). b) Map of high latitude rivers analyzed and permafrost extent. Locations of high latitude rivers analyzed for bank erosion rates shown in red. The permafrost map shows zones of permafrost extent from isolated to continuous (Obu et al., 2019 version 2.0).

3.1.2 Pan-Arctic satellite and aerial photo analysis.

We generated a new dataset of riverbank erosion rates across the northern high latitudes ($\geq 60^\circ$ N) on 13 Arctic and sub-Arctic rivers with varying permafrost conditions, sizes, and morphologies (Rowland & Stauffer, 2019b). The rivers included: the Yukon, Selawik, Koyukuk, Noatak, and Colville Rivers in Alaska, and the Indigirka, Kolyma, Lena, Ob, Pechora, Taz, Yana, and Yenesei River in Russia (Figure 2b). We supplemented our analysis with river masks generated by Brown et al. (2020) for the lower Yukon, Tanana, and Chandalar Rivers in Alaska. The drainage area of the analyzed rivers ranged between 1,300 km² (Selawik) and 2.5 x 10⁶ km² (Yenisei); widths ranged between 65 m (Selawik) and 6,500 m (Lena); and planform morphologies varied from single-threaded meandering to multi-threaded braided and anastomosing. All river sections analyzed were bounded by alluvial floodplains. Based on published maps of permafrost distributions, all rivers have some degree of permafrost in their watersheds and along the river channels (Brown et al., 2002; Gruber, 2012; Obu et al., 2018, 2019; Pastick et al., 2013, 2015) (Figure 2b).

We used 129 images from the Landsat archive, higher resolution satellite imagery, and aerial photography collected between the 1970s and 2018 to generate binary masks of more than 5,500 km high latitude rivers (Table S1) (Rowland & Stauffer, 2019a). The masks were generated using the automated feature extraction software GeniePro (Perkins et al., 2005) and eCognition (Flanders et al., 2003). Masks of the bankfull channel extent, not subject to variations in river stage at the time of image acquisition, were generated by classifying both water and bare, vegetation-free sediment along the banks and channel islands as part of the active channel (Donovan et al., 2019; Rowland et al., 2016 and references therein). The masks were analyzed using the Spatially Continuous Riverbank Erosion and Accretion Measurements (SCREAM) software (Rowland et al., 2016). A detailed description of both the SCREAM methodology for measuring erosion rates and channel widths may be found in Rowland *et al.* (2016). All masks were manually inspected and corrected for errors generated by shadows, clouds, and poor classifications prior to analysis with SCREAM.

The accuracy and comparability of SCREAM generated erosion rates to results derived from other published methodology used to measure erosion rates on non-Arctic rivers was presented in Rowland *et al.* (2016). In addition, we used SCREAM to measure the erosion rates for three lower latitudes rivers, (the Ucayali River, Peru, the Strickland River, Papua New Guinea, and the East River, Colorado) that span a broad range of drainage areas. The results of these measurement are both consistent with the published data for these rivers (Aalto et al., 2008; J Schwenk et al., 2017) and do not show a bias compared to the complete low latitude dataset.

We averaged individual bank measurements along sections of rivers to compare reach scale rates to watershed properties, such as drainage area, sediment yield, discharge, slope and permafrost, and to weight measurements between rivers proportionately. We created bins based on changes in upstream drainage area, such that the drainage area associated with each new river segment increased by 20% on average with a minimum increase of 5%. For rivers which had multiple time periods of analyses, such as the Yukon, Lena, Koyukuk, and Noatak Rivers, we used only the longest time interval in our global comparison, resulting in a dataset of 78 measurements.

Errors in individual measurements of erosion rates and channel width were quantified in Rowland et al. (2016). The largest source of error comes from the ability to accurately classify the location of a riverbank in remotely sensed imagery. Rowland et al. (2016) estimated that the error in bank erosion measurements for any time interval, due to bank classification, was 0.35

pixels. Therefore, the shorter the time interval over which change is measured the greater the error in erosion rates. In this study, we used the standard error (SE) of the mean based on the reach-averaging discussed above which incorporates the measurement uncertainty into the reach-scale measurements.

Donovan et al. (2019) provided an in-depth evaluation of the importance of and methods for incorporating detection limits into the reporting of remotely sensed river migration rates. Here, we assigned a value of zero to all erosion measurements below the threshold of detection. We confirmed that this approach did not lead to image resolution dependent results by comparing rates measured with 30 m Landsat imagery to rates measured with high-resolution imagery over approximately the same time intervals (Supporting Text S3 and Figure S4).

To assess other sources of error and bias in our dataset, we tested the influence of river planform morphology and measurement time interval on erosion rates (Donovan & Belmont, 2019 and references therein). The hypothesis that the erosion measurements from single- and multi-threaded rivers come from the same distributions could not be rejected using two-tailed Wilcoxon rank sum tests for either high or low latitude rivers (Figure S5). Moreover, there was not a statistically significant correlation between erosion rates and measurement time intervals present in either of our datasets (Figure S6).

3.1.3 Analysis of remotely sensed and published erosion rates

We conducted two comparisons of high and low latitude erosion rates. First, we normalized all erosion rates by channel width to control for the general trend of increasing erosion rates with river size (Hooke, 1980; Ielpi & Lapôtre, 2020; Krasnoshchekov, 2009; van de Wiel, 2003). The measurements were compared across the full datasets, and separately by reach averaged and locally based erosion rates. Wilcoxon rank-sum test between the datasets were performed with a significance threshold set at 0.05.

Second, we compared high and low latitude erosion rates by examining the relationships between erosion rate and stream power (Ω):

$$\Omega = \gamma QS, \quad (1)$$

where, γ is the specific weight of water (the density of water (ρ) times gravity (g)), Q is the discharge, and S is the river slope. Prior studies have found stream power to be an effective predictor of bank erosion (Akhtar et al., 2011; Bizzi & Lerner, 2015; Hickin & Nanson, 1984; Larsen et al., 2006; Lawler et al., 1999; Moody, 2022; Nanson & Hickin, 1986). Stream power incorporates both hydrological variability through discharge and basin characteristics through slope.

The selection of an appropriate value for Q (eq 1) requires determining what discharge values are both relevant to bank erosion and comparable across rivers. Numerous studies have shown that the onset of bank erosion correlates to a critical value of boundary shear stress and hence discharge (Darby et al., 2010; Francalanci et al., 2020; Leyland et al., 2015; Rinaldi et al., 2008; Rinaldi & Darby, 2008). This threshold value is often associated with a bankfull discharge which commonly is assigned based on flow frequency analysis and a specific return interval (Bizzi & Lerner, 2015; Naito & Parker, 2019). Recent modeling suggests that a range of high but not extreme flows may provide a more meaningful hydrological predictor for channel dynamics (Naito & Parker, 2019, 2020).

Few bank erosion studies reported bankfull or maximum discharges, and many of the rivers in both our Arctic and meta-analysis of published erosion rates are ungauged or lack reliable stream flow data for the reaches of interest. Therefore, we extracted the long-term

average (1960 – 2015) of the FLO1K annual maximum monthly discharge (Barbarossa et al., 2018) using the Python package rabpro (J Schwenk et al., 2022). The annual maximum monthly captures both geomorphically relevant discharges that occur for sufficient durations to be effective and avoids biases of short-lived outliers potentially captured in the annual maximum daily discharge.

In our regression analysis of erosion rates, we sought to address two potential sources of uncertainty and bias. First, our datasets have non-uniform errors in erosion rates, and second, our measurements were not uniformly distributed across stream power, raising the possibility that linear regressions to the datasets could be influenced by outliers. To address these issues, we used a boot-strap method for regression. We randomly sampled with replacement 5,000 subsets of the original stream power – erosion rate data pairs. Each of the 5,000 subsets were the same length as the two original datasets (high and low latitude). For each randomly selected stream power value an erosion rate was randomly selected from a normal distribution of erosion rates constructed from the mean erosion rate and a standard deviation equal to the standard error of the mean erosion rate. We then log10-transformed both the randomly selected stream power and erosion rate values and fit a linear regression to the transformed data. From the 5,000 regressions we obtained a distribution of mean slopes, intercepts, r^2 , p -values, and values corresponding to the 95th confidence intervals that incorporate the uncertainty in erosion rate measurements and tests the possible influence of outliers. The influence of outliers was minimized because no single sample retained all of the original values in the dataset. On average, 63% of the original stream power-erosion pairs were included in any individual sample, the maximum percentage of the dataset in any sample was 70%.

3.1.4 Analysis of the influence of river hydrology and sediment load

To test alternative hypotheses that hydrology could explain differences in erosion rates between permafrost influenced and permafrost free rivers we used global hydrological databases of river discharges (Land2Sea dataset (L2S) (Peucker-Ehrenbrink, 2009) and (Dai & Trenberth, 2002)). We evaluated whether strong seasonality of peak river flows leads to relatively inefficient bank erosion due to the potential non-linear (< 1) relationship between river discharge and shear stresses driving bank erosion such that greater time-integrated erosion rates for the same total annual discharge under differing hydrographs. We modeled erosion rates along the Yukon and Lena Rivers by redistributing the total annual flows for the Yukon and Lena River based on the hydrographs of nine lower-latitude rivers that spanned seven climate zones and had stream powers ranging from 1,400 to 4,000 W m^{-1} (Supporting Text S4).

We used a widely applied excess boundary shear stress model of bank erosion that does not attempt to account for bend specific hydrodynamic controls on erosion rates (Darby et al., 2007; Francalanci et al., 2020; Midgley et al., 2012; Partheniades, 1965; Pizzuto, 2009; Zhao et al., 2022):

$$E = \kappa_d (\tau_b - \tau_c)^\alpha \quad (2)$$

where E is the linear erosion per unit time, κ_d is an erodibility coefficient with units of $\text{m}^3/\text{N/s}$, τ_b and τ_c are the boundary and critical shear stress for initiation of bank erosion in Pa, respectively, and α is a dimensionless exponent commonly set to 1 (Rinaldi & Darby, 2007; Zhao et al., 2022). Parameterization of Eq 2 and data sources for the Yukon and Lena Rivers is presented in Supporting Text S5.

3.2 Field observations and measurements

We conducted field investigations along two rivers (Yukon and Koyukuk) in the boreal forest region of Alaska (Young et al., 2017) and one river (Selawik) in tussock tundra dominated western Alaska (Raynolds et al., 2019).

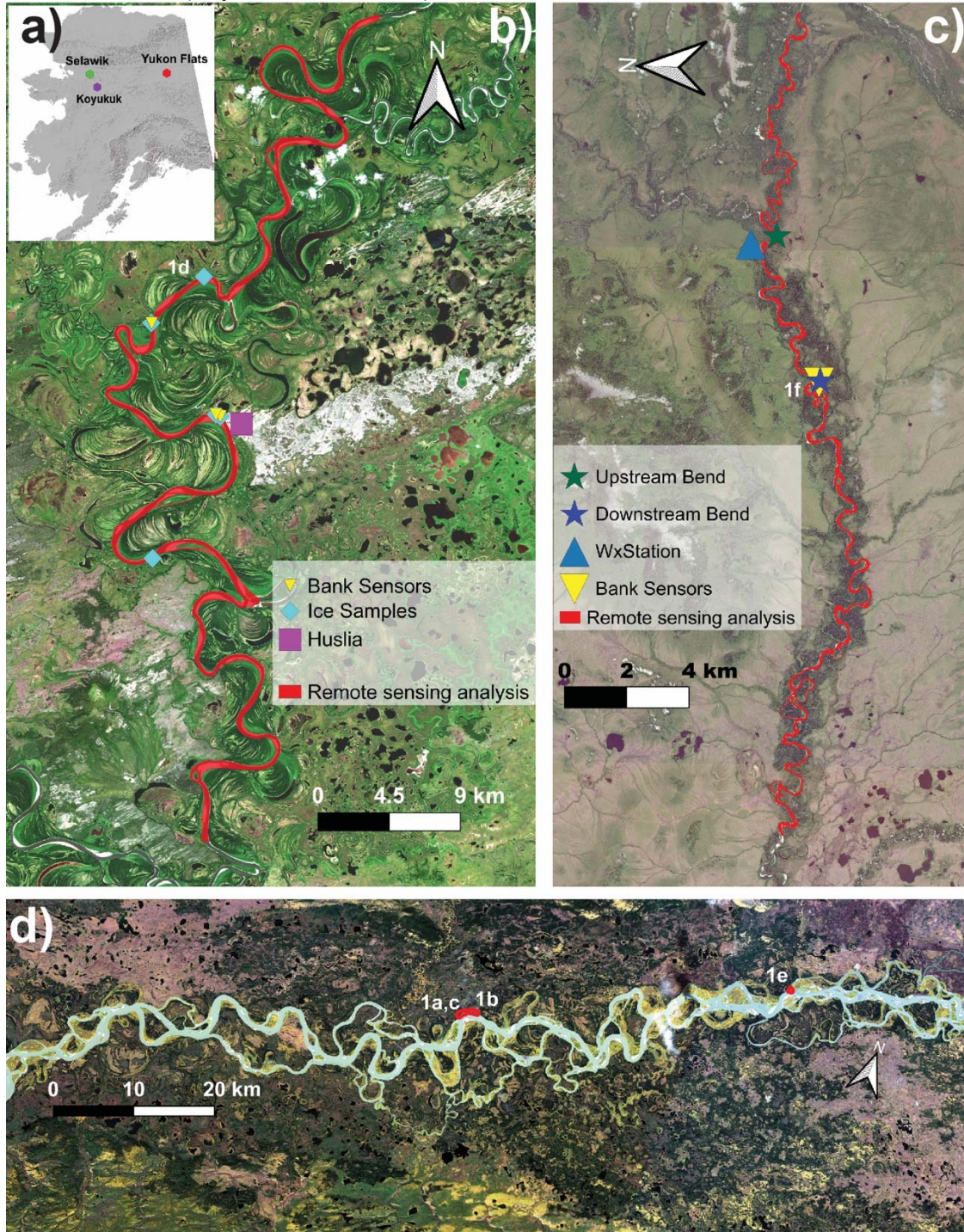


Figure 3: Field study locations. **a)** Locations of three rivers where field observations were collected. **b)** Koyukuk River with measurement locations highlighted. Background image is a Sentinel 2 scene acquired in July 2022. The river flow is from north to south. Location of image in Figure 1d annotated. **c)** Selawik River study reach with locations of sensors and bends discussed in text highlighted. Background is an August 2, 2022 Worldview3 image (©2022 Maxar). The river flows from east to west. Location of image in Figure 1f annotated. **d)** Section of Yukon

River in the Yukon Flats where field observations were made in 2009. Red outlines with labels indicate location of images in Figure 1. Remote sensing analysis include this entire reach and extended both up- and downstream. Background image is a Sentinel 2 scene acquired in July 2022.

3.2.1. Koyukuk River, Alaska

We conducted field work on the Koyukuk River near the Village of Huslia (65.7 N, 156.4 W) in 2018. This section of the Koyukuk River flows through an extensive floodplain up to 18 km wide that is located south of the Brooks Range and north of the river's confluence with the Yukon River. The Koyukuk drains 80,000 km² upstream of the study reach. The mean annual discharge at the Hughes gauging station (66.0475, -154.258), located just upstream of the study reach averaged 406 m³/s between 1961 and 1981

(https://waterdata.usgs.gov/nwis/inventory/?site_no=15564900). Along this section, the Koyukuk is primarily a single-threaded and meandering sand bed river. The floodplain is composed of sandy deposits overlain by silty fines with scroll bar complexes easily visible due to the coincidence of curvilinear rows of trees. At the village of Huslia, a site of pronounced local erosion in permafrost-free aeolian bluffs, residents have reported average riverbank erosion rates of 3-9 m/yr, with a yearly maximum of 30 m in 2004 and episodic rates of erosion as high as 18 m in a single spring flood in 2003 (U.S. Army Corps of Engineers, 2007).

Vegetation on the floodplain is heterogeneous with willow in early successional areas along the river such as point bars and a mix of black spruce, white spruce, and aspens along older floodplain regions and scroll bar complexes. Treeless expanses of old oxbows and drained lakes are covered by grasses and generally lacking permafrost. Mosses and tundra vegetation overlay older deposits with permafrost. Both field observations and published maps (Obu et al., 2019; Pastick et al., 2015) indicate that the floodplain is underlain by discontinuous permafrost with strong correlations between vegetation cover and the presence of near surface permafrost. Ice content in frozen sediments is highly variable with excess ground ice commonly observed in drained lake basins. Based on the Climatic Research Unit (CRU) 0.5° data, the mean annual temperature at Huslia was -5.3° C between 1978 and 2018, with a 0.03°/yr increase in mean annual temperature over that time period (Harris et al., 2020).

Field work on the Koyukuk River was conducted in June and July of 2018. Surveys to determine the location and extent of permafrost consisted of coring, digging pits, trenching of cutbank faces, and a visual inspection of banks from a boat to note distinctive permafrost features (e.g., overhanging tundra mats, thermoerosional niching, ice wedges, active drainage of ice melt from soils). Coring locations were chosen based on where permafrost was suspected to be present or absent and to sample a range of geomorphic units and relative deposit ages based on scroll bar and meander patterns preserved on the floodplain. Coring was conducted using a SIPRE corer, designed to core into frozen soils. Cores were 1-2 m in length and the presence of permafrost was inferred by the existence of frozen soil at depth. We also conducted more extensive permafrost surveys using a soil probe to note the presence or absence of frozen ground in the upper 1 m of soil (the length of the probe). These observations and multispectral WorldView 3 (WV3) imagery acquired in May 2018, and an interferometric synthetic aperture radar (IfSAR) data were used to train a convolutional neural network model (CNN) to predict the occurrence of permafrost across the study site (Schwenk et al., 2023).

At exposed bank faces, thawed sediment was removed, and the underlying frozen bank was inspected to characterize grain size, stratigraphy, and ice structures. A concrete corer 210 ml in volume was used to extract frozen samples from the exposed bank face at 11 locations across five banks to measure bulk density and ice content. We used the pvlib python package

(Holmgren et al., 2018) to calculate the average annual total direct solar irradiance at each of these five riverbanks. Riverbank temperatures were monitored at five locations along 3 riverbanks using an array of iButton loggers installed in a custom rod manufactured by Alpha Mach Inc. The temperature loggers were located at the bank face, 5, 10, 20, and 40 cm depths (Rowland et al., 2023).

3.2.2 Selawik River, Alaska

The Selawik River flows east to west on the southern side of the Kiliovilik Range on the southern margin of the Brooks Range. Field research was conducted in the vicinity of an actively eroding retrogressive thaw slump (Barnhart & Crosby, 2013) near the confluence with the Kiliovilik Creek, Alaska (66.49 N, -157.60 W) in 2010, 2011, and 2012. Along the study reach the drainage area ranges from 1,100 to 2,000 km² and the average channel width is 65 m. The largely single-threaded river has a gravel bed with filled and partially filled abandoned channel segments occupying a floodplain approximately 1 km in width. The Selawik River is ungauged but modelled river discharges estimate a long-term mean annual discharge of 27 m³/s (Barbarossa et al., 2018).

The region is characterized by shrubby tussock tundra with birch and willows along river and stream corridors (Cable et al., 2016; Jorgenson et al., 2009). Mean annual air and one meter deep soil temperatures near our study sites were reported as -4.6 and -3.9 C, respectively (Cable et al., 2016). Though mapped at the transition between discontinuous and sporadic permafrost zones (Obu et al., 2019; Pastick et al., 2015), we observed permafrost to be present along most of the floodplain except for active and newly abandoned point bar deposits and gravel-dominated channel fills with overlying silt deposits less than 40 cm thick. Observations of excess ground ice were limited to isolated ice wedges exposed in eroding hillslopes and lowland surfaces topographically above the present-day floodplain.

Soil and air temperatures on the Selawik were recorded at hourly time intervals (Rowland et al., 2023). Soil temperature sensors were placed 50 cm below the ground surface at 66.48 N, 157.71 W. Air temperatures were recorded at two meters above the ground surface at a weather station located 5 km upstream (66.500 N, 157.609 W).

3.2.3 Yukon River, Alaska

We conducted field work in the Yukon Flats of central Alaska near the Village of Beaver (66.3594, -147.3964) in the summer of 2009. This reach has been classified as a wandering planform morphology (Clement, 1999) and features multiple threads with a few dominant channels and large stable islands. An upstream drainage area of 500,000 km² generates a mean annual discharge of 3,450 m³/s measured at the stream gauge located at the downstream end of the study reach (https://waterdata.usgs.gov/nwis/inventory/?site_no=15453500). In this section of river, the total width varies from 1,500 and 2,700 m. The bed material is dominated by gravel. Riverbanks ranging in height from four to six meters are composed of gravel in the lower half and overlain by sandy overbank deposits, and a reported slope of 0.0001 (Clement, 1999).

4 Results

In the following sections, we present results from the largest spatial (pan-Arctic and global) and temporal (decades) scales and progressively decrease in magnitude to examine riverbank erosion at the smallest spatial (riverbank) and temporal (days) scales.

4.1. Pan-Arctic erosion rates relative to low latitude rivers systems.

Rivers with permafrost showed a clear and statistically significant difference in width normalized erosion rates relative to rates measured in permafrost-free watersheds (Figure 4a; two-tailed Wilcoxon rank sum tests ($p\text{-value} < 0.001$)). Erosion rates grouped by reach scale measurements indicated that permafrost-influenced rivers had normalized erosion rates 5.7 times lower (0.006 ± 0.001 versus 0.034 ± 0.003 , mean \pm standard error). Grouped across all measurements and for local scale measurements, high latitude rivers had mean normalized erosion rates with statistically significant lower rates.

The non-normalized reach-scale bank erosion rates for both high and low latitude rivers show a correlation with the estimated stream power for each river reach (Figure 4b). For each dataset, we plotted the mean best-fit regression along with all the individual boot-strapped linear regressions within the 95th confidence interval for the slope (shown as shaded regions). The mean best-fit regression yielded statistically significant ($p\text{-value} < 0.01$) power law relationships for both sets of riverbank erosion rates: low latitude $E = 0.008(0.014/0.005)\Omega^{0.77(0.85/0.68)}$; high latitude $E = 0.19(0.36/0.09)\Omega^{0.23(0.31/0.16)}$ (the numbers in parentheses are the values of the upper and lower 95th confidence intervals). Stream power proved a stronger predictor of bank erosion rates in low latitude ($r^2 = 0.58$) than high latitude ($r^2 = 0.27$) rivers. None of the 5,000 boot-strapped regressions yielded slopes for either dataset that overlapped with the other.

None of the high latitude rivers for which we measured erosion rates had stream powers lower than the point of intersection of the two regression lines ($\Omega \sim 350 \text{ W m}^{-1}$). We plotted the four lowest stream power data points (diamonds) in the dataset of previously published rates (all based on local studies). Two locations fall above the intersection of regression lines and two below; the ones below plot on the same regression line as the low latitude dataset. We also marked (black triangles) three low latitude rivers we analyzed with the SCREAM methodology to highlight that the trend of our high latitude dataset does not appear to be an artifact of the analysis method.

A pan-Arctic comparison of erosion rates to published maps of permafrost (Brown et al., 2002; Gruber, 2012; Obu et al., 2018, 2019) does not show a correlation between erosion rates and the relative extent of permafrost in the basin or individual river reaches. Our evaluation of these permafrost products (Supporting Text S6) showed high uncertainties regionally particularly in areas of variable permafrost such as floodplains. For example, in the Yukon Flats region of Alaska, a local permafrost map and a state-wide data product produced by the same research group had significant disagreement at the scale of individual river reaches and bends (Pastick et al., 2014, 2015). Therefore, at the pan-Arctic scale we can only conclude that rivers with some extent of permafrost have lower reach-averaged bank erosion rates compared to rivers with equivalent stream power in basins without permafrost. The difference in erosion rate is up to 40 times at stream powers of $400,000 \text{ W m}^{-1}$ but becomes insignificant at stream powers less than $1,000 \text{ W m}^{-1}$.

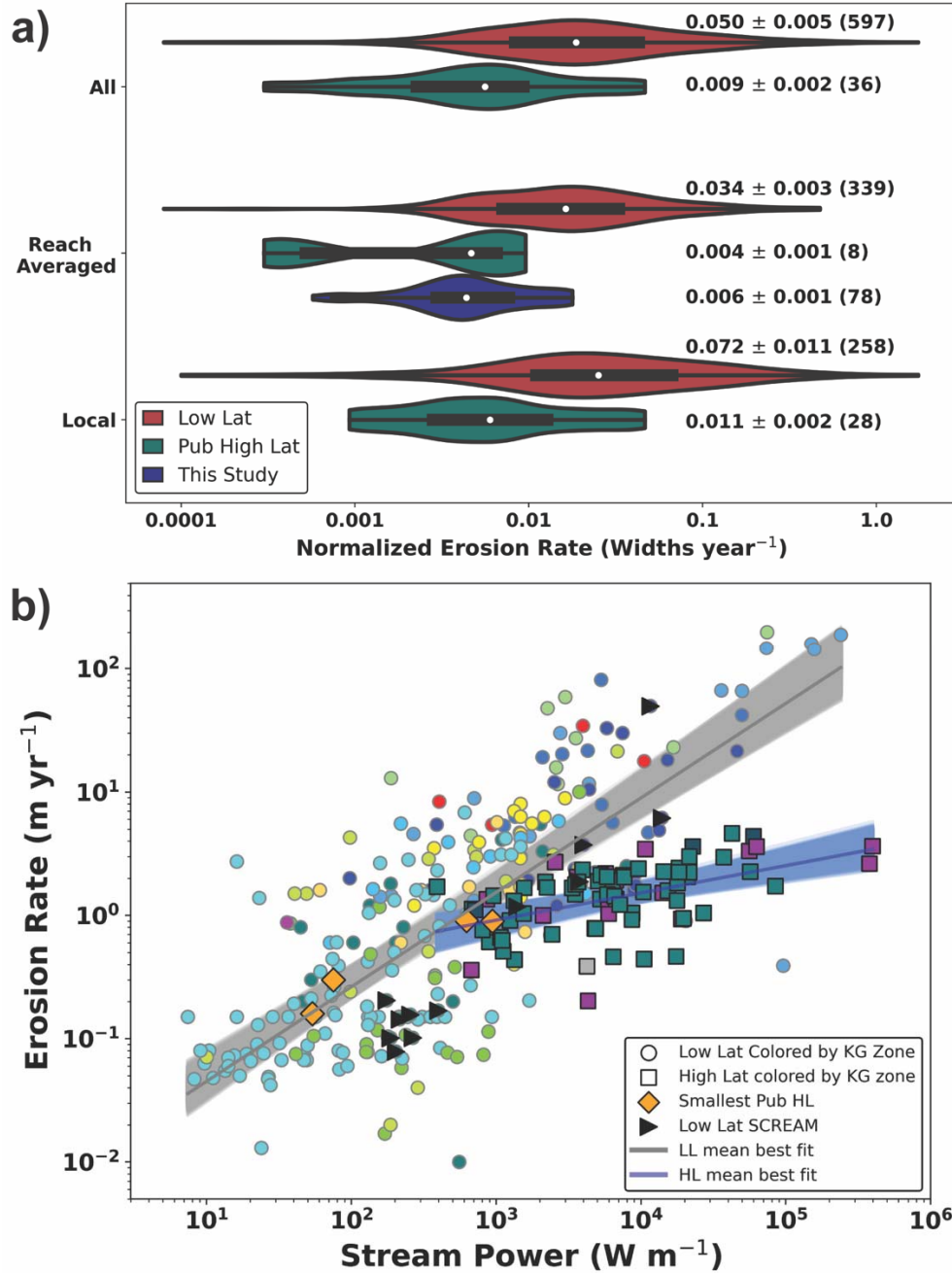


Figure 4: Comparisons of high and low latitude riverbank erosion rates. a) Violin plots of width-normalized riverbank erosion rates for high and low latitude rivers. These plots show the range and distribution of bank erosion rates from published data and our analyses. The y-axis indicates three categories: “All”-data regardless of the scale of measurement, “Reach-averaged” measurements, and “Local” measurements (point to bend-scale). The black rectangles display the interquartile range, the lines indicate the 1.5x interquartile range, white dots represent median values. The numbers report the mean, standard error, and number of observations (in parentheses). b) Reach-averaged erosion rates plotted by stream power. Circular points are data compiled from published studies and squares are high latitude rivers analyzed in this study. All points are colored by the Köppen-Geiger climate zones (Beck et al., 2018) shown in Figure 2a. The solid gray and blue lines show the mean best fit regressions from the 5,000 boot-strapped linear fits to the log10 transformed data. The shaded regions show all the regressions that fell within the 95th confidence intervals based on the distributions of modeled slopes. Diamond symbols show the published erosion rates of rivers with the smallest stream powers.

4.2 Riverbank permafrost and ice content on the Koyukuk River

4.2.1 Reach and bend erosion rate variations with permafrost extent

Using the permafrost map we generated for the Koyukuk River (Section 3.2.2) (Figure 5), we found that erosion rates averaged over 10-channel width long segments showed a general trend in decreasing erosion rates as the fraction of permafrost in the surrounding floodplain increased from 0.23 to 0.72 (Figure 6a). Erosion rates averaged at the individual bend scale (Figure 6b) also showed clear correlation between permafrost extent and decreases in erosion rates.

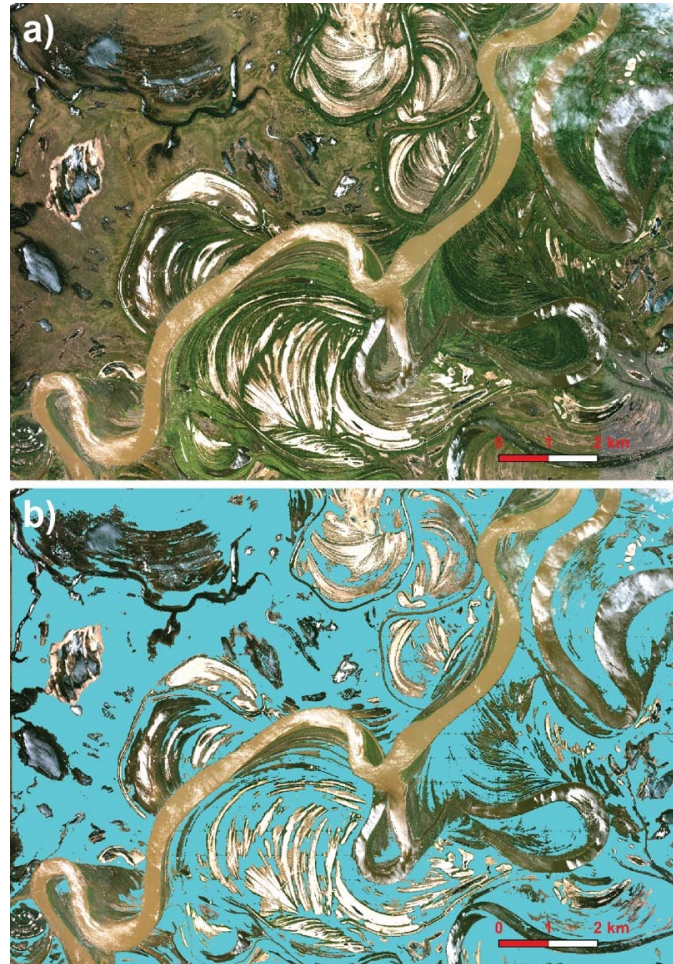


Figure 5: Example segment of permafrost map generated for the Koyukuk River, AK. **a)** May 2018 Worldview3 image of the Koyukuk River just upstream of the Village of Huslia (©2018 Maxar). **b)** mapped permafrost extent (blue) of the Koyukuk River floodplain.

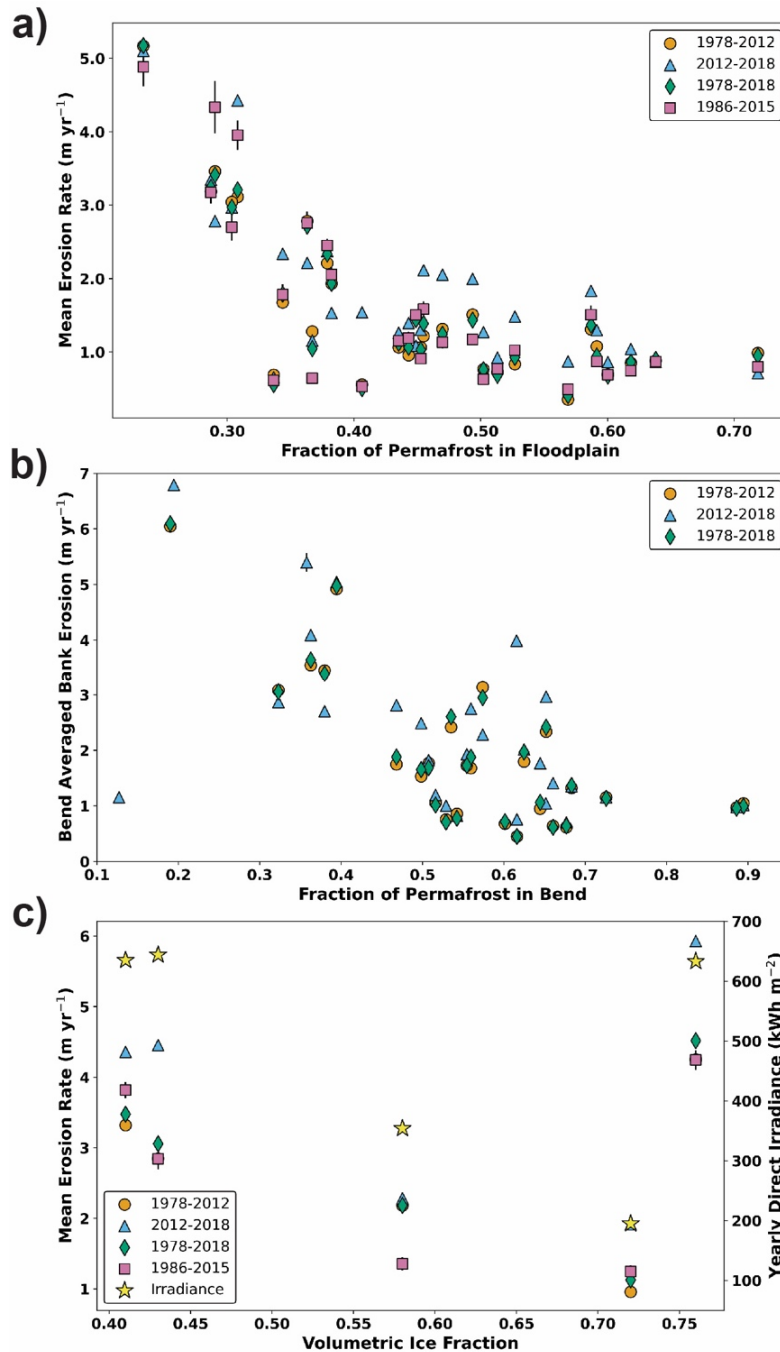


Figure 6: **a)** Riverbank erosion rates averaged along segments approximately 10 channel widths in length on the Koyukuk River, AK, plotted against the fraction of permafrost mapped in the surrounding floodplain. Linear regressions were significant at p -values < 0.01 for all time periods, the r^2 values were 0.52, 0.49, 0.51 and 0.50 for 1978-2012, 2012-2018, 1978-2018, and 1986-2015, respectively. **b)** Riverbank erosion rates averaged over outer banks on individual bends along the Koyukuk River, AK, plotted against the fraction of permafrost mapped in the surrounding floodplain. Linear regressions were significant at p -values < 0.01 for all time periods, the r^2 values were 0.54, 0.33 and 0.54 for 1978-2012, 2012-2018, and 1978-2018, respectively. **c)** Erosion rates of individual riverbank segments (left vertical axis) plotted by the volumetric ice content of bank material and the modeled yearly solar irradiance received by the bank (right vertical axis). In all plots, the vertical lines on the points show the standard errors of the erosion rates, where not visible the SE is smaller than the symbol.

4.2.2 Bank erosion rates and volumetric ice content

Volumetric ice content at five bends we sampled on the Koyukuk River ranged from 0.41 to 0.76 (Rowland et al., 2023). Erosion rates decreased with increasing ice content at four of the five locations (Figure 6c); the fifth location had the highest ice content and exhibited the highest erosion rates. Of the two locations with the highest ice contents (0.72 and 0.76), the location with the lowest erosion rates faced almost due north (321°) and the one with the highest rates faced almost due south (179°). A comparison of the total annual irradiance to erosion rates and ice content (Figure 6c righthand vertical axis) showed that the rapidly eroding, high-ice content, south-facing bank, received approximately three times as much direct solar radiation as the north-facing, high ice content bank. The rapidly eroding bank showed clear evidence of thermal denudation in the field with water generated by melting ice causing active slumping of the fine-grained banks and subaerial retreat (Figure 1d). A comparison of erosion rates to annual direct irradiance at all bends in this section of the Koyukuk River, however, suggests that irradiance alone is not a strong predictor of erosion rates, even in banks with large fractions of permafrost (Figure S8).

4.3 Bank material properties and temperature profiles on the Selawik River

Erosion rates measured between 1981 and 2009 along a 45 km reach of the Selawik River averaged 0.68 ± 0.03 m/yr (all rates are the mean and standard error) and ranged from 0 to 5.7 m/yr. This range highlights the spatial variability commonly observed across the full permafrost-affected river erosion dataset (J. C. Rowland & Stauffer, 2019b). To explore controls on this variability, we collected field observations and analyzed seven years of 2 m resolution satellite imagery at two bends 5 km apart. The bends had equivalent hydrology, similar width-normalized radii of curvature (2.6 vs 2.7), and both were eroding permafrost-dominated floodplains. Despite these similarities, one bend (shown in Figure 1f) had a 28-year averaged erosion rate of 3.90 ± 0.11 m/yr and the other 0.40 ± 0.07 m/yr (Figure 7a).

Bend-averaged erosion rates between 2009 and 2016 at the rapidly eroding bend ranged from non-detectable to 4.65 ± 0.66 m/yr (Figure 7a). Only two of these years had erosion rates close to or exceeding the longer-term average. Field observations indicate that most of the annual bank erosion occurred in a few days of snowmelt-driven flows during the spring. We observed total erosion of 5.4 m in one section of this bend in the spring of 2011, 63% of which occurred over less than four days.

The temperature sensor data from the rapidly eroding riverbank (Rowland et al., 2023) led us to infer that the bank remained frozen until the bank materials collapsed into the river. On May 25, 2011, the temperature sensor originally installed 2 m from the eroding bank face recorded an abrupt increase in temperature from -0.16 to 4°C between hourly measurements and then ceased recording data (Figure 7b). We interpret the jump in temperature to reflect the sensor encountering river water just prior to the sensor being lost. A nearby sensor, initially located 7 m from the bank face, buried at the same depth recorded a ground temperature of -0.9°C , indicating that sediments in the proximity of the bank face remained frozen throughout this time period.

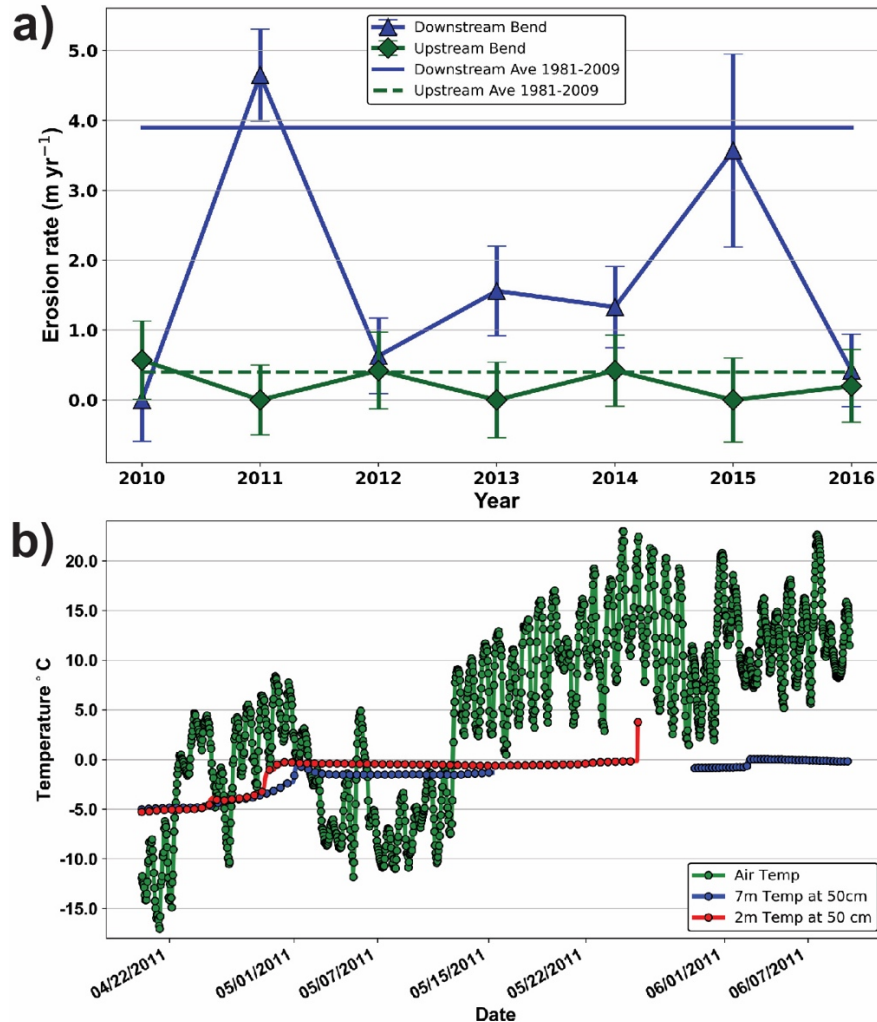


Figure 7: Erosion rates and thermal conditions of riverbanks along the Selawik River, AK. a) Bend averaged erosion rates for two bends at yearly intervals from 2010 to 2016. Horizontal lines indicate the long-term (1981-2009) erosion rates for each bend. Error bars show the standard error of the erosion rates. b) Air and riverbank soil temperatures at the downstream river bend shown in a). Hourly soil temperature data collected at a depth of 50 cm, initially located 2 and 7 m from the riverbank face (the 7 m sensor was 1.6 m from the bank face at the end of May 2011). In May 2011, bank erosion exposed the 2 m temperature sensor (red) to river water prior to the sensor being lost and data collection ending. Plot markers for the soil temperatures are only displayed every 12 hours for visibility. Local air temperatures are plotted in green to highlight the spring warming. Figure 1f shows the downstream bend where the bank temperatures were recorded (panel b).

This bend exhibited little to no erosion during times of lower river discharge throughout the ice-free season despite abundant loose gravels mantling the bank face and toe. During this period, blocks of tussock tundra that had collapsed following high snowmelt flow-driven bank undercutting (Figure 1f) appeared to help protect the bank from erosion even during late-season, rainfall-induced high flows of similar magnitude to snowmelt flow. Despite their persistence following high summer flows, these blocks were not present following ice-break up in the spring.

Remotely sensed, yearly measurements of bank erosion rates between 2009 and 2016 at the slowly eroding upstream bend, ranged from non-detectable to 0.57 ± 0.56 m/yr (Figure 7a). Unlike the gravel dominated, rapidly eroding downstream bend, this bank was composed of fine

to medium sand, and tussock tundra covered its face. Our excavation of the bank face revealed that this tundra was associated with failure blocks that had collapsed and refrozen to the underlying sandy deposits. These blocks appeared to remain fixed to the bank throughout the spring ice-out flows and were extremely difficult to remove during bank excavation.

4.4 Subaerial thaw and retreat of riverbanks, and river ice-driven erosion

In addition to the thermal degradation of the ice-rich, south facing riverbank on the Koyukuk (Figure 1d), we observed both transient and persistent subaerial thaw and retreat of riverbanks along both the Yukon and Koyukuk Rivers. Along both rivers, frozen bank materials were exposed at the bank face immediately following the recession of high flows and at locations where steep bank geometry prevented the accumulation of thawed sediments (Figure 1a). Following flow recession, subaerially exposed bank sediments appeared to thaw rapidly. On the Koyukuk River we installed five temperature sensor arrays horizontally at bank locations with high ice contents composed of silty sediments (corresponding to the 0.57 ice content location of Figure 6c), and lower ice content fine to medium sands (two lowest ice content points on Figure 6c). Prior to installing the temperature arrays, we removed all thawed sediment down to frozen materials. Over the course of two weeks in the late June and early July 2018, the banks thawed between 40 to 124 mm/day with rates generally decreasing with higher ice contents (Rowland et al., 2023). In all locations, the thawed materials remained in place and created a thermal buffer between the diurnally fluctuating air temperatures and the advancing thaw front. This buffer reduced the thaw rate by 40% between the 0 to 10 cm and the 10 to 20 cm distances from the bank face.

Along both the Yukon and Koyukuk Rivers, subaerial portions of the exposed vertical bank faces and the undersides of thaw niches continued to retreat even when not directly exposed to river water. This retreat occurred as thawing chunks of bank material spalled off the subaerial face and dropped into the flowing river and were carried away from the bank face (Figure 1a). Along banks with extensive thermal niches on the Yukon River massive failure blocks that were 10 m wide and several meters thick were observable in July 2009 (Figure 1b). Despite their size, the blocks appeared to thaw rapidly, and rarely appear in high-resolution imagery persisting from one year to the next. Shallowly rooted trees and tundra tended to detach and slide off the tilted blocks (Figure 1b) offering limited bank protection from further erosion.

In June/July 2009 we observed one additional mechanism for non-fluvial bank erosion on the Yukon River in the Yukon Flats. At a limited number of locations concentrated at the head of islands several decimeters of sediment were removed from the floodplain surface during spring ice out, as if scraped off by a bulldozer (Figure 1e). The ice-impacted bank sections appeared spatially limited on the Yukon and potentially had a minimal effect on the lateral retreat of the riverbanks.

5 Discussion

Our pan-Arctic analysis showed that rivers in basins with permafrost on average have width-normalized bank erosion rates six times lower than non-permafrost rivers (Figure 4a). This rate difference increased with river size and stream power from negligible to 40 times at the highest stream powers (Figure 4b). The results from the Koyukuk River suggest that permafrost concentration has a significant control on variations in bank erosion rates for this river with robust linear decreases in erosion rates as permafrost in the riverbanks increases (Figure 6). With the uncertainty of permafrost data available across the Arctic (Supporting Text S6) we do not

have clear evidence for similar relationship at the pan-Arctic scale. While across all rivers we see significant variation in the range of erosion rates for given permafrost fractions, we do observe clear upper bounds on the maximum rates of erosion. We interpret these results to indicate that locally many factors control bank erosion rates, but permafrost systematically sets an upper limit on these rates.

Despite our findings that permafrost exerts a strong control on riverbank erosion, prior research has suggested that other characteristics of permafrost-affected rivers may have equal or greater control on riverbank erosion rates than permafrost. Therefore, we examined three possible alternative hypotheses to assess the hypothesis that permafrost is the dominant control of lower erosion rates observed in high latitude rivers.

5.1. Alternative hypothesis 1: shorter annual flow durations in northern rivers result in comparatively less flow relative to basin size.

Given the short duration over which Arctic rivers flow, these rivers may have less total discharge relative to basin drainage area than comparable low latitude rivers. Despite the strong seasonality of discharge in northern high latitude rivers (Church, 1977; Holmes, Coe, et al., 2012; Woo et al., 2008) a comparison of the total annual discharge versus drainage basin size showed no clear distinction between high and low latitude systems (Figure 8a). We analyzed the linear relationship between total annual discharge and drainage basin size using the Land2Sea dataset (L2S) (Peucker-Ehrenbrink, 2009). The paired *t*-test of the slopes (Zar, 1999) indicated that the relationship between total annual discharge and drainage basin size did not differ between high and low latitude systems (*p*-value = 0.2; Figure 8a). The Amazon River was excluded from this analysis because it is a global outlier, even within low latitude systems (Milliman & Farnsworth, 2013). The null hypothesis that the specific water yields (annual river discharge divided by drainage basin area) for high and low latitude rivers come from the same populations cannot be rejected by a two-tailed *t*-test (*p*-value = 0.9). An evaluation using the Dai & Trenberth (2002) datasets yielded identical results (Figure S9). We thus conclude that differences in flow volumes between high and low latitude rivers are not likely responsible for the discrepancy in erosion rates.

5.2. Alternative hypothesis 2: Shorter but larger flow peaks result in less efficient erosion.

The second alternative hypothesis is that the extreme seasonality of peak Arctic river flows leads to relatively inefficient bank erosion due to the potential non-linear (< 1) relationship between river discharge and shear stresses driving bank erosion. That is, rivers with flow distributed more evenly in time may have greater time-integrated erosion rates for the same total annual discharge. Using our modeled erosion rates (Section 3.1.5, Figure 8b, Supporting Text S5) we found that in most cases the modeled total erosion using the flatter hydrographs equaled or exceeded the modeled erosion using natural hydrographs for both the Yukon and Lena (Figure 8c). The magnitude of erosion increases (27% maximum), however, failed to explain the 40 times greater erosion rates observed on lower latitude rivers of equivalent drainage areas (Figure 4b), thus we rejected the second hydrological hypothesis for lower erosion rates for high latitude rivers.

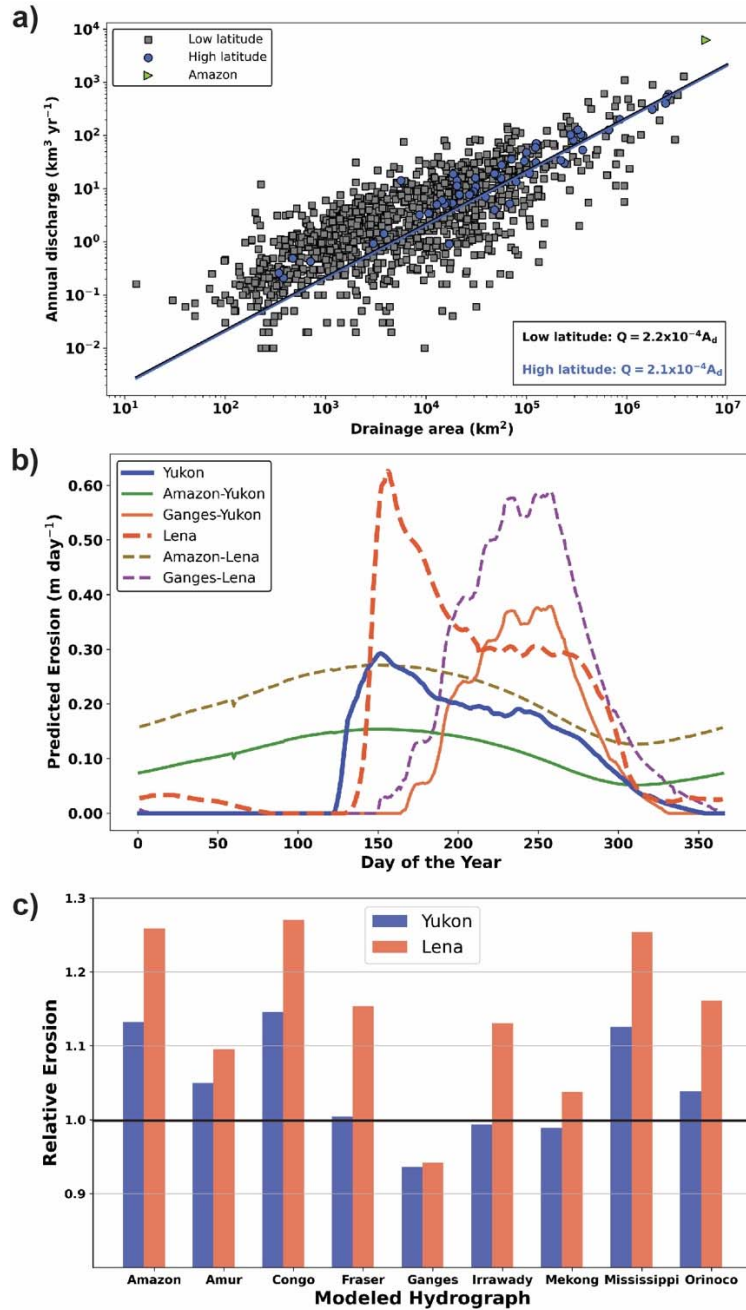


Figure 8: Comparisons low and high latitude river basin hydrology. **a)** Data from Land2Sea (Peucker-Ehrenbrink, 2009) separated into high ($n = 54$) and low ($n = 1203$) latitude river systems and plotted with annual discharge (Q) versus drainage area (A_d). Linear regression lines for both high (blue) and low latitude (black) are plotted, but the black line is obscured by the blue line. The r^2 of the regressions are 0.96 for high latitude and 0.55 for low latitude rivers (p -values < 0.001). **b)** Modeled daily erosion using Eq 2 for both the Yukon and Lena Rivers. The plot shows erosion based on observed long-term averaged daily flow for each river and for the same annual volume of flow temporally redistributed for two large low latitude rivers with high bank erosion rates and stream powers. **c)** Predicted erosion for the Yukon and Lena Rivers using observed total annual discharge temporally distributed based on the average annual hydrographs of nine lower-latitude rivers. Values greater than one indicate that modeled erosion would be greater if the annual flow for the Yukon or Lena Rivers were redistributed in time equivalent to the lower-latitude river's flow regime.

The rejection of alternative hypotheses 1 and 2 suggest that differences in hydrology between northern high latitude rivers and other river systems are not adequate to singularly explain the regional differences in erosion rates. The power-law regressions in Figure 4b also indicated that stream power (hydrology) has much less predictive power for bank erosion in high latitudes ($r^2 = 0.27$) than for river systems without permafrost ($r^2 = 0.58$).

5.3 Alternative hypothesis 3: Lower sediment loads in high latitude rivers lead to lower bank erosion rates.

Previous studies have suggested that riverbank erosion rate increases with a river's sediment load (Dietrich et al., 1999; Dunne et al., 1981, 2010; Torres et al., 2017). This is supported by the positive correlations between sediment loads and rates of lateral channel migration documented along rivers in the Amazon basin (Constantine et al., 2014), and in laboratory experiments (Bufe et al., 2016; Wickert et al., 2013). These observations led us to explore whether the observed differences in erosion rates could be explained by the significantly lower sediment loads measured in high latitude rivers as compared to lower latitude systems (Gordeev, 2006) (Figure 9a). However, a comparison of erosion rates showed no correlation between width-normalized erosion rates and sediment yield either by latitude grouping or globally (Figure 9b). We also found no correlation between modeled sediment yields (Cohen et al., 2013) and erosion rates for river reaches in our datasets (Figure S10).

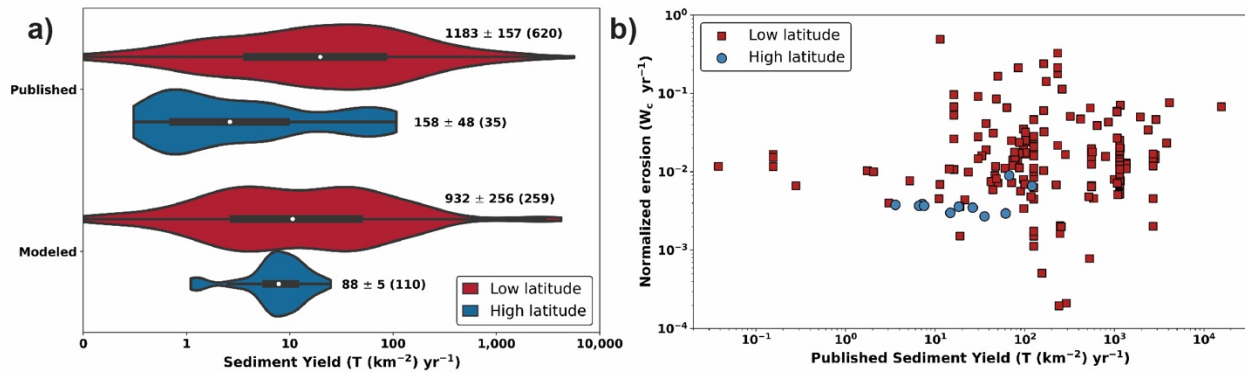


Figure 9: Comparison of low and high latitude sediment yields and associated erosion rates. **a)** Violin plots of published and modeled long-term average sediment yields (Cohen et al., 2013). The published data represent a combination of values reported in the L2S dataset (Peucker-Ehrenbrink, 2009) and values published elsewhere in the literature (Rowland & Schwenk, 2019). The rectangles display the interquartile range, the lines indicate the 1.5x interquartile range, white dots represent median values, and the displayed numbers are the mean, standard error, and number of observations (in parentheses). **b)** Width-normalized erosion rates versus published sediment yield data.

The absence of a correlation between erosion rate and sediment yields does not rule out that sediment loads may influence riverbank erosion rates. However, based on the best available data, we conclude that it is unlikely that differences in sediment loads between high and low latitude rivers provides a compelling alternative to permafrost as the dominant control on observed discrepancy in erosion rates.

5.4 A stream power transition for permafrost influence on riverbank erosion rates

The regression lines for erosion rates as a function of stream power for high and low latitudes intersect at a stream power of 350 Wm^{-1} . This stream power value corresponds roughly

to rivers less than 60 m wide or drainage areas $\sim 1,000 \text{ km}^2$ (Figure S7). Given the uncertainty in the regression and variability in the data, we suggest that a change in scaling between high and low latitude system occurs over a transition between 350 and $\sim 900 \text{ W m}^{-1}$ (drainage areas 1,000 to $10,000 \text{ km}^2$) and we hypothesize that the scaling relationship observed for our high latitude dataset does not extend below values of 350 W m^{-1} . Below this transition, our observations suggest that erosion rates of rivers in permafrost settings may become largely transport limited such that bank retreat rates are limited by the occurrence of flows sufficient to mobilize already-thawed sediments. Above this threshold, maximum bank erosion rates are limited by the rate at which frozen bank material may be thawed. The only two published studies of permafrost-affected rivers on systems with stream powers $< 350 \text{ W m}^{-1}$ suggests that small Arctic rivers may have similar erosion dependence on stream power as we observed at lower latitudes.

In our high latitude dataset, the Selawik River lies closest to this stream power transition. On this river we observe both transport and thaw-limited controls on bank erosion rates. At the rapidly eroding bank highlighted in Figure 7a and shown in Figure 1f, riverbank eroded less material than thaws seasonally in many years; a similar observation was made for the Usuktuk River in northern Alaska (Matsubara et al., 2015). Additionally, there exists a supply of readily transportable gravels throughout most of the summer, but few summer flows appear to be able to mobilize these sediments. In years of significant snowmelt-driven spring flooding, such as 2011, high transport rates appear to fully exhaust the supply of unfrozen bank materials and the thaw rate sets the upper limit of bank retreat (Figure 7b). On the Selawik River, the timing and rate of erosion also appear to be locally influenced by the bank grain size distributions and the presence and preservation of vegetated failure blocks. River ice may play a key role in removing these detached failure blocks and allowing renewed erosion of the banks.

Both the grain size of riverbanks and peak flow characteristics correlate to river basin size in ways that are consistent with smaller rivers being more transport limited and larger rivers having a greater thermal control on erosion rates. Generally, bank materials become finer with larger upstream drainage basin areas (Knighton, 2014) and therefore a broader range of flows may be capable of transporting loose sediment away from thawing banks reducing erosion dependence on transport conditions and increasing the relative importance of thermal controls. Ice content also tends to be higher in finer grained sediments (French & Shur, 2010). In many settings, increasing ice content slows bank erosion rates (Figure 6c) (Randriamazaoro et al., 2007; Shur et al., 2002; J. R. Williams, 1952b), rendering riverbanks more thermally limited. Smaller rivers in the Arctic tend to have flashier hydrographs as measured by the ratio of maximum to mean annual discharges (Figure S11). Coarser, flashier, small rivers and streams likely erode under transport limited threshold conditions set by bankfull or peak flows (Naito & Parker, 2019, 2020).

5.5 Scale-dependent response of riverbank erosion to changing climate in the Arctic.

Our multi-temporal analysis of erosion rates was limited to a few rivers and time periods, limiting our ability to assess changes in riverbank erosion rates due to historical climate forcings. We performed multi-temporal analyses on the Yukon, Koyukuk, Noatak, and Lena Rivers but observed no clear pattern of temporal trends of rates greater than the observed interannual variability. On the Koyukuk River, however, analysis of high-resolution imagery provided differences erosion rates greater than our levels of detection. Even though climate data for this region indicates that a 1°C increase in mean annual air temperature occurred between the time periods of our erosion analysis (1978-2012 and 2012-2018) (Harris et al., 2020) the temporal

trends in rates were inconclusive; higher erosion rates occurred during the most recent time interval (2012 – 2018) at some but not all the sections and bends examined (Figure 8).

Potential climate drivers for changes in riverbank erosion rates in regions of permafrost include temperature, hydrology, sediment loads, and changes in river ice. In recent decades the Arctic has warmed three times faster than the rest of the planet (AMAP, 2021) and is projected to continue to warm (Cai et al., 2021). Strong correlations between air and river temperatures (Yang & Peterson, 2017) portend increases in river temperatures and subsequent acceleration of riverbank thaw rates for rivers that are presently thaw limited ($> 900 \text{ W m}^{-1}$, Figure 4b).

Projections suggest that hydrologically, northern rivers will shift from a nival (snowmelt) to more pluvial (rainfall) regime (Woo, 1990) with an increase in late summer flows (Lafrenière & Lamoureux, 2019) and extreme events (Nilsson et al., 2015). On larger rivers, a shift from snow melt dominated flow regimes to higher summer flows will combine with increased river temperatures to accelerate thermal erosion of banks (Dupeyrat et al., 2011). Floods may remove thawed bank materials more effectively and expose frozen banks to greater thermal erosion. A flattening of peak flows and more even distribution of discharge over the summer may also increase erosion on the largest of Arctic rivers (Section 5.2, Figure 8c). On smaller rivers a decrease in peak flows below critical thresholds for erosion may reduce bank erosion unless offset by larger magnitude summer floods.

We do not have enough confidence in the rate or magnitude of changes in future sediment fluxes to speculate how important these changes will be to riverbank erosion. In a recent review, Zhang et al. (2022) highlight that changes in sediment loading to rivers may vary greatly in space and time depending on the drivers of sediment production.

Finally, a future reduction in winter ice cover (Chassiot et al., 2020) may reduce erosion rates across rivers of all sizes. On large rivers, abrasion and scour from local ice-jam flooding should decrease (Lininger & Wohl, 2019). On small rivers, less ice may leave protective failure blocks intact through the peak snowmelt floods and reduce bank erosion. For example, on the Selawik River we observed 10 times greater erosion rates on bends where blocks were removed versus bends where blocks remained in place during major spring flows (Figure 7a).

6 Conclusions

For over forty years researchers have been unable to conclusively determine if permafrost influences the rate of riverbank erosion relative to rivers without permafrost. Based on the pan-Arctic analysis, global meta-analysis of riverbank erosion, and field observations we found a statistically significant six times lower mean width normalized erosion rate along riverbanks with permafrost compared to riverbanks lacking permafrost. At stream powers of < 350 to 900 W m^{-1} (upstream drainage areas 1,000 to 10,000 km^2), we observed no difference between high and low latitude rivers. Above this transition in stream power, however, the differences in erosion rates increases to a factor of 40 for the largest rivers in our datasets.

We conclude that it is most likely that permafrost is the foremost control on the relatively low bank erosion rates of high latitude rivers based on direct evidence from the Koyukuk River and a rejection of potential alternative hypotheses. Data from the Koyukuk River showed a reach and bend scale reduction in erosion rates as the fraction of permafrost in the surrounding floodplain increased. A lack of high-resolution and reliable permafrost maps at the pan-Arctic scale precluded a similar analysis along and between other rivers.

In both our pan-Arctic dataset and detailed observations along individual rivers, erosion rates vary greatly even between banks with equivalent permafrost extent, however, the presence

of permafrost does appear to set an upper limit on the maximum erosion rates. We suggest that this maximum limit is set by the rate at which frozen bank material may thaw and provide loose sediment for transport. Thermal sensors installed in a bend along the Selawik River, AK appears to confirm this thaw limitation. Our data further suggests that this thaw limitation on bank erosion transitions to a transport limitation for rivers with stream powers below 350 to 900 W m⁻¹.

This apparent transition from thaw- to transport-limited erosion may exert a significant control on how rivers will respond to climate change in the Arctic. The erosion rates of thermally limited riverbanks of large rivers will likely increase as river temperatures increase and flow shifts from snowmelt dominated to higher discharges during the warmer summer months. Conversely, smaller transport-limited rivers may experience a decrease in erosion rates with a reduction in peak snow melt flows, unless these peak flows become offset by high-magnitude rain driven floods. A decrease in river ice will likely also reduce erosion rates on both large and small rivers, but it is unlikely that at the watershed to pan-Arctic-scale such reduction in large rivers will offset the anticipated increases in thermally driven erosion rates. Riverbank erosion represents a significant direct risk to communities and infrastructure and associated changes in sediment and nutrient loading will likely impact fisheries and water quality. Our ability to predict and mitigate such impacts, however, will require additional data with higher spatial and temporal resolutions to better constrain permafrost extent and the mechanics, drivers, and timing of riverbank erosion in permafrost-affected floodplains.

Acknowledgements

Primary funding for this research was provided by the U.S. Department of Energy Office of Science Biological and Environmental Research Earth and Environmental Systems Sciences Division Early Career Award to J. Rowland, and the Regional and Global Model Analysis Program funded Interdisciplinary Research for Arctic Coastal Environments (InterFACE) project. Additional funding was provided by Los Alamos National Laboratory Laboratory Directed Research and Development for the work on Selawik River. Other funding sources for co-authors was provided by Caltech Terrestrial Hazards Observation and Reporting Center, Foster and Coco Stanback, the Linde Family, and the Resnick Sustainability Institute to Michael P. Lamb; National Science Foundation Awards 2127442 and 2031532; the National Defence Science and Engineering Graduate Fellowship for Madison M. Douglas and Preston C. Kemeny; and the Fannie and John Hertz Foundation Cohen/Jacobs and Stein Family Fellowship for Preston C. Kemeny. We thank the U.S. Fish and Wildlife Service Selawik National Wildlife Refuge for logistical support. Dana Brown, Mitchell Donovan, and Marc Van De Wiel provided data that supported the compilation of erosion rates. Logistical support was provided by Shawn Huffman, Alvin Attla, and Virgil Umphenour for work on the Koyukuk River. We thank the Koyukuk-hotana Athabascans, First Chief Norman Burgett, and the Huslia Tribal Council for access to their land and USFWS–Koyukuk National Wildlife refuge for research permitting and logistical assistance.

Open Research

All original data and software used in this manuscript have been archived at the DOE ESS-DIVE data portal (<http://ess-dive.lbl.gov/>) and are cited and referenced in the manuscript.

References

- Aalto, R., Lauer, J. W., & Dietrich, W. E. (2008). Spatial and temporal dynamics of sediment accumulation and exchange along Strickland River floodplains (Papua New Guinea) over decadal-to-centennial timescales. *J. Geophys. Res.*, 113(Journal Article), F01S04.
- Akhtar, M. P., Sharma, N. A. Y. A. N., & Ojha, C. S. P. (2011). Braiding process and bank erosion in the Brahmaputra River. *International Journal of Sediment Research*, 26(4), 431–444. [https://doi.org/10.1016/S1001-6279\(12\)60003-1](https://doi.org/10.1016/S1001-6279(12)60003-1)
- AMAP. (2021). *Arctic Climate Change Update 2021: Key Trends and Impacts. Summary for Policy-makers*. Tromsø, Norway.
- Are, F. E. (1983). Thermal abrasion of coasts. In *Proceedings of the Fourth International Conference on Permafrost* (pp. 24–28).
- Barbarossa, V., Huijbregts, M. A. J., Beusen, A. H. W., Beck, H. E., King, H., & Schipper, A. M. (2018). Data Descriptor: FLO1K, global maps of mean, maximum and minimum annual streamflow at 1 km resolution from 1960 through 2015. *Scientific Data*, 5(February), 180052. <https://doi.org/10.1038/sdata.2018.52>
- Barnhart, T. B., & Crosby, B. T. (2013). Comparing two methods of surface change detection on an evolving thermokarst using high-temporal-frequency terrestrial laser scanning, Selawik River, Alaska. *Remote Sensing*, 5(6), 2813–2837. <https://doi.org/10.3390/rs5062813>
- Beck, H. E., Zimmermann, N. E., McVicar, T. R., Vergopolan, N., Berg, A., & Wood, E. F. (2018). Present and future köppen-geiger climate classification maps at 1-km resolution. *Scientific Data*, 5, 1–12. <https://doi.org/10.1038/sdata.2018.214>
- Bizzi, S., & Lerner, D. N. (2015). The use of stream power as an indicator of channel sensitivity to erosion and deposition processes. *River Research and Applications*, 31(1), 16–27.
- Blume-Werry, G., Milbau, A., Teuber, L. M., Johansson, M., & Dorrepaal, E. (2019). Dwelling in the deep – strongly increased root growth and rooting depth enhance plant interactions with thawing permafrost soil. *New Phytologist*, 223(3), 1328–1339. <https://doi.org/10.1111/nph.15903>
- Brinkman, T. J., Hansen, W. D., Iii, F. S. C., Kofinas, G., Burnsilver, S., & Rupp, T. S. (2016). Arctic communities perceive climate impacts on access as a critical challenge to availability of subsistence resources. *Climatic Change*, 413–427. <https://doi.org/10.1007/s10584-016-1819-6>
- Brown, D. R. N., Brinkman, T. J., Bolton, W. R., Brown, C. L., Cold, H. S., Hollingsworth, T. N., & Verbyla, D. L. (2020). Implications of climate variability and changing seasonal hydrology for subarctic riverbank erosion. *Climatic Change*, 162, 385–404. <https://doi.org/10.1007/s10584-020-02748-9>
- Brown, J. O., Heginbottom, J. A., & Melnikov. (2002). Circum-Arctic Map of Permafrost and Ground-Ice Conditions, Version 2. Boulder, Colorado USA: NSIDC: National Snow and Ice Data Center. <https://doi.org/10.7265/skbg-kf16>
- Bufe, A., Paola, C., & Burbank, D. W. (2016). Fluvial bevelling of topography controlled by lateral channel mobility and uplift rate. *Nature Geoscience*, 9(9), 706–+. <https://doi.org/10.1038/ngeo2773>
- Cable, W. L., Romanovsky, V. E., & Torre Jorgenson, M. (2016). Scaling-up permafrost thermal measurements in western Alaska using an ecotype approach. *Cryosphere*, 10(5), 2517–2532. <https://doi.org/10.5194/tc-10-2517-2016>

- Cai, Z., You, Q., Wu, F., Chen, H. W., Chen, D., & Cohen, J. (2021). Arctic warming revealed by multiple CMIP6 models: Evaluation of historical simulations and quantification of future projection uncertainties. *Journal of Climate*, 34(12), 4871–4892. <https://doi.org/10.1175/JCLI-D-20-0791.1>
- Chassiot, L., Lajeunesse, P., & Bernier, J. F. (2020). Riverbank erosion in cold environments: Review and outlook. *Earth-Science Reviews*, 207(June), 103231. <https://doi.org/10.1016/j.earscirev.2020.103231>
- Church, M. (1977). River studies in Northern Canada: reading the record from river morphology. *Geoscience Canada*, 4(1), 4–12.
- Clement, D. T. (1999). *Fluvial Geomorphology of the Yukon River, Yukon Flats, Alaska. Geography*.
- Cohen, S., Kettner, A. J., & Syvitski, J. P. M. (2013). WBMsed, a distributed global-scale riverine sediment flux model : Model description and validation. *Computers & Geosciences*, 53, 80–93. <https://doi.org/10.1016/j.cageo.2011.08.011>
- Cold, H. S., Brinkman, T. J., Brown, C. L., Hollingsworth, T. N., Brown, D. R. N., & Heeringa, K. M. (2020). Assessing vulnerability of subsistence travel to effects of environmental change in Interior Alaska. *Ecology and Society*, 25(1).
- Constantine, J. A., Dunne, T., Ahmed, J., Legleiter, C., & Lazarus, E. D. (2014). Sediment supply as a driver of river meandering and floodplain evolution in the Amazon Basin. *Nature Geoscience*, 7(12), 899–903.
- Cooper, R. H., & Hollingshead, A. B. (1973). River bank erosion in regions of permafrost. In *Proceedings of the Hydrology Symposium* (Vol. 9, pp. 272–283). Edmonton, Alberta: Subcommittee on Hydrology by the Inland Waters Directorate, Department of the Environment.
- Costard, F., Dupeyrat, L., Gautier, E., & Carey-Gailhardis, E. (2003). Fluvial thermal erosion investigations along a rapidly eroding river bank: application to the Lena River (central Siberia). *Earth Surface Processes and Landforms*, 28(12), 1349–1359. Retrieved from <http://dx.doi.org/10.1002/esp.592>
- Costard, F., Gautier, E., Brunstein, D., Hammadi, J., Fedorov, A., Yang, D., & Dupeyrat, L. (2007). Impact of the global warming on the fluvial thermal erosion over the Lena River in Central Siberia. *Geophysical Research Letters*, 34(14), L14501.
- Costard, F., Gautier, E., Fedorov, A., Konstantinov, P., & Dupeyrat, L. (2014). An assessment of the erosion potential of the fluvial thermal process during ice breakups of the Lena River (Siberia). *Permafrost and Periglacial Processes*, 25(3), 162–171.
- Dai, A., & Trenberth, K. E. (2002). Estimates of freshwater discharge from continents: Latitudinal and seasonal variations. *Journal of Hydrometeorology*, 3(6), 660–687. [https://doi.org/10.1175/1525-7541\(2002\)003<0660:eofdfc>2.0.co;2](https://doi.org/10.1175/1525-7541(2002)003<0660:eofdfc>2.0.co;2)
- Darby, S. E., & Thorne, C. R. (1996). Development and testing of riverbank-stability analysis by Stephen E. Darby 1 and Colin R. Thorne,2 Affiliate Member, ASCE. *Journal of Hydraulic Engineering*, 122(August), 443–454.
- Darby, S. E., Rinaldi, M., & Dapporto, S. (2007). Coupled simulations of fluvial erosion and mass wasting for cohesive river banks. *Journal of Geophysical Research-Earth Surface*, 112(F3). <https://doi.org/10.1029/2006jf000722>
- Darby, S. E., Trieu, H. Q., Carling, P. A., Sarkkula, J., Koponen, J., Kumm, M., et al. (2010). A physically based model to predict hydraulic erosion of fine-grained riverbanks: The role of

form roughness in limiting erosion. *Journal of Geophysical Research: Earth Surface* (2003–2012), 115(F4).

Debol'skaya, E. I., & Ivanov, A. v. (2020). Comparative Analysis of Models of Thermoerosion-Induced Channel Deformations in Rivers of Permafrost Zone. *Water Resources*, 47(1), 77–86. <https://doi.org/10.1134/S0097807820010054>

Dietrich, W. E., Day, G., & Parker, G. (1999). The Fly River, Papua New Guinea: Inferences about River Dynamics, Floodplain Sedimentation and Fate of Sediment. In *Varieties of Fluvial Forms* (pp. 345–376). New York: John Wiley & Sons Ltd.

Dingle, E. H., Sinclair, H. D., Venditti, J. G., Attal, M., Kinnaird, T. C., Creed, M., et al. (2020). Sediment dynamics across gravel-sand transitions: Implications for river stability and floodplain recycling. *Geology*, 48(5), 468–472. <https://doi.org/10.1130/G46909.1>

Donovan, M., & Belmont, P. (2019). Timescale dependence in river channel migration measurements. *Earth Surface Processes and Landforms*, 44(8), 1530–1541. <https://doi.org/10.1002/esp.4590>

Donovan, M., Belmont, P., Notebaert, B., Coombs, T., Larson, P., & Souffront, M. (2019). Accounting for uncertainty in remotely-sensed measurements of river planform change. *Earth-Science Reviews*, 193(April), 220–236. <https://doi.org/10.1016/j.earscirev.2019.04.009>

Donovan, M., Belmont, P., & Sylvester, Z. (2021). Evaluating the Relationship Between Meander-Bend Curvature, Sediment Supply, and Migration Rates. *Journal of Geophysical Research: Earth Surface*, 126(3), 1–20. <https://doi.org/10.1029/2020JF006058>

Douglas, M. M., Li, G. K., Fischer, W. W., Rowland, J. C., Kemeny, P. C., West, A. J., et al. (2022). Organic carbon burial by river meandering partially offsets bank erosion carbon fluxes in a discontinuous permafrost floodplain. *Earth Surface Dynamics*, 10(3), 421–435.

Drake, T. W., Guillemette, F., Hemingway, J. D., Chanton, J. P., Podgorski, D. C., Zimov, N. S., & Spencer, R. G. M. (2018). The Ephemeral Signature of Permafrost Carbon in an Arctic Fluvial Network. *Journal of Geophysical Research: Biogeosciences*, 123(5), 1475–1485. <https://doi.org/10.1029/2017JG004311>

Dunne, T., Dietrich, W. E., Humphrey, N. F., & Tubbs, D. W. (1981). Geologic and geomorphic implications for gravel supply. In *Proceedings of the Conference on Salmon-Spawning Gravel: A Renewable Resource in the Pacific Northwest* (pp. 75–100).

Dunne, T., Constantine, J. A., & Singer, M. (2010). The role of sediment transport and sediment supply in the evolution of river channel and floodplain complexity. *Transactions, Japanese Geomorphological Union*, 31(2), 155–170.

Dupeyrat, L., Costard, F., Randriamazaoro, R., Gailhardis, E., Gautier, E., & Fedorov, A. (2011). Effects of ice content on the thermal erosion of permafrost: Implications for coastal and fluvial erosion. *Permafrost and Periglacial Processes*.

Eardley, A. J. (1938). Yukon Channel Shifting. *Bulletin of the Geological Society of America*, 49, 343–358.

Ettema, R. (2002). Review of Alluvial-channel Responses to River Ice. *Journal of Cold Regions Engineering*, 16(4), 191–217. [https://doi.org/10.1061/\(ASCE\)0887-381X\(2002\)16:4\(191\)](https://doi.org/10.1061/(ASCE)0887-381X(2002)16:4(191))

Flanders, D., Hall-Beyer, M., & Pereverzoff, J. (2003). Preliminary evaluation of eCognition object-based software for cut block delineation and feature extraction. *Canadian Journal of Remote Sensing*, 29(4), 441–452. <https://doi.org/10.5589/m03-006>

- Francalanci, S., Lanzoni, S., Solari, L., & Papanicolaou, A. N. (2020). Equilibrium Cross Section of River Channels With Cohesive Erodible Banks. *Journal of Geophysical Research: Earth Surface*, 125(1), 1–20. <https://doi.org/10.1029/2019JF005286>
- French, H. (2007). *The Periglacial Environment* (Vol. 3). Hoboken: John Wiley & Sons, Ltd. Retrieved from <http://alamos.ebib.com/patron/FullRecord.aspx?p=291041>
- French, H., & Shur, Y. (2010). The principles of cryostratigraphy. *Earth-Science Reviews*, 101(3–4), 190–206. <https://doi.org/10.1016/j.earscirev.2010.04.002>
- Gatto, L. W. (1984). *Tanana River monitoring and research program: relationships among bank recession, vegetation, soils, sediments and permafrost on the Tanana River near Fairbanks, Alaska* (Vol. 84). US Army Corps of Engineers, Cold Regions Research and Engineering Laboratory.
- Gautier, E., Dépret, T., Cavero, J., Costard, F., Virmoux, C., Fedorov, A., et al. (2021). Fifty-year dynamics of the Lena River islands (Russia): Spatio-temporal pattern of large periglacial anabranching river and influence of climate change. *Science of The Total Environment*, 783, 147020. <https://doi.org/10.1016/j.scitotenv.2021.147020>
- Gordeev, V. v. (2006). Fluvial sediment flux to the Arctic Ocean. *Geomorphology*, 80(1–2), 94–104. <https://doi.org/10.1016/j.geomorph.2005.09.008>
- Gruber, S. (2012). Derivation and analysis of a high-resolution estimate of global permafrost zonation. *Cryosphere*, 6(1), 221–233. <https://doi.org/10.5194/tc-6-221-2012>
- Gustafsson, O., van Dongen, B. E., Vonk, J. E., Dudarev, O. v., & Semiletov, I. P. (2011). Widespread release of old carbon across the Siberian Arctic echoed by its large rivers. *Biogeosciences*, 1737–1743. <https://doi.org/10.5194/bg-8-1737-2011>
- Harris, I., Osborn, T. J., Jones, P., & Lister, D. (2020). Version 4 of the CRU TS monthly high-resolution gridded multivariate climate dataset. *Scientific Data*, 7(1), 109. <https://doi.org/10.1038/s41597-020-0453-3>
- Hickin, E. J., & Nanson, G. C. (1984). Lateral migration rates of river bends. *Journal of Hydraulic Engineering*, 110(11), 1557–1567.
- Hinzman, L. D., Kane, D. L., & Woo, M. (2005). Permafrost Hydrology. In M. Anderson (Ed.), *Encyclopedia of Hydrological Sciences* (Vol. 4, pp. 2679–2693). West Sussex, U. K.: John Wiley.
- Holmes, R. M., Coe, M. T., Fiske, G. J., Gurtovaya, T., McClelland, J. W., Shiklomanov, A. I., et al. (2012). Climate change impacts on the hydrology and biogeochemistry of Arctic rivers. In C. R. Goldman, M. Kumagai, & R. D. Robarts (Eds.), *Climatic change and global warming of inland waters: Impacts and mitigation for ecosystems and societies* (1st ed., pp. 1–26). John Wiley & Sons, Ltd. <https://doi.org/10.1002/9781118470596.ch1>
- Holmes, R. M., McClelland, J. W., Peterson, B. J., Tank, S. E., Bulygina, E., Eglinton, T. I., et al. (2012). Seasonal and annual fluxes of nutrients and organic matter from large rivers to the Arctic Ocean and surrounding seas. *Estuaries and Coasts*, 35(2), 369–382. <https://doi.org/10.1007/s12237-011-9386-6>
- Holmgren, W. F., Hansen, C. W., & Mikofski, M. A. (2018). pvlib python: a python package for modeling solar energy systems. *Journal of Open Source Software*, 3(29), 884. <https://doi.org/10.21105/JOSS.00884>
- Hooke, J. M. (1980). Magnitude and distribution of rates of river bank erosion. *Earth Surface Processes*, 5(2), 143–157.

1095 Hovelsrud, G. K., Poppel, B., van Oort, B., & Reist, J. D. (2011). Arctic societies, cultures, and
 1096 peoples in a changing cryosphere. *Ambio*, 40(SUPPL. 1), 100–110.
 1097 <https://doi.org/10.1007/s13280-011-0219-4>
 1098 Ielpi, A., & Lap tre, M. G. A. (2020). A tenfold slowdown in river meander migration driven by
 1099 plant life. *Nature Geoscience*, 13(1), 82–86. <https://doi.org/10.1038/s41561-019-0491-7>
 1100 Instanes, A., Kokorev, V., Janowicz, R., Bruland, O., Sand, K., & Prowse, T. (2016). Changes to
 1101 freshwater systems affecting Arctic infrastructure and natural resources. *Journal of*
 1102 *Geophysical Research-Biogeosciences*, 121(3), 567–585.
 1103 <https://doi.org/10.1002/2015jg003125>
 1104 Jackson, R. B., Canadell, J., Ehleringer, J. R., Mooney, H. A., Sala, O. E., & Schulze, E. D.
 1105 (1996). A global analysis of root distributions for terrestrial biomes. *Oecologia*, 108(3),
 1106 389–411. <https://doi.org/10.1007/BF00333714>
 1107 Jorgenson, M. T., Roth, J. E., Miller F., P., Macander, M. J., Duffy, M. S., Wells, A. F., et al.
 1108 (2009). *An Ecological Land Survey and Landcover Map of the Selawik National Wildlife*
 1109 *Refuge. Natural Resource Technical Report.*
 1110 Kanevskiy, M., Shur, Y., Strauss, J., Jorgenson, T., Fortier, D., Stephani, E., & Vasiliev, A.
 1111 (2016). Patterns and rates of riverbank erosion involving ice-rich permafrost (yedoma) in
 1112 northern Alaska. *Geomorphology*, 253, 370–384.
 1113 <https://doi.org/10.1016/j.geomorph.2015.10.023>
 1114 Knighton, D. (2014). *Fluvial forms and processes: a new perspective*. Routledge.
 1115 Krasnoshchekov, S. Y. (2009). *Determining lateral river channel activity with respect to safety*
 1116 *of pipeline crossings*. University of Southampton.
 1117 Lafreni re, M. J., & Lamoureux, S. F. (2019). Effects of changing permafrost conditions on
 1118 hydrological processes and fluvial fluxes. *Earth-Science Reviews*, 191(June 2018), 212–
 1119 223. <https://doi.org/10.1016/j.earscirev.2019.02.018>
 1120 Larsen, E. W., Premier, A. K., & Greco, S. E. (2006). Cumulative Effective Stream Power and
 1121 Bank Erosion on the Sacramento River, California, USA. *Journal of the American Water*
 1122 *Resources Association*, 42(4), 1077–1097. [https://doi.org/10.1111/j.1752-](https://doi.org/10.1111/j.1752-1688.2006.tb04515.x)
 1123 [1688.2006.tb04515.x](https://doi.org/10.1111/j.1752-1688.2006.tb04515.x)
 1124 Lawler, D. M., Grove, J. R., Couperthwaite, J. S., & Leeks, G. J. L. (1999). Downstream change
 1125 in river bank erosion rates in the Swale–Ouse system, northern England. *Hydrological*
 1126 *Processes*, 13(7), 977–992.
 1127 Lawson, D. E. (1983). *CRREL Report 83-29 Erosion of perennially frozen streambanks* (83rd–
 1128 29th ed.). Hanover, N.H.
 1129 Leffingwell, E. K. (1919). *The Canning River region, northern Alaska. USGS Professional*
 1130 *Paper 109*. Washington, D.C.
 1131 Leyland, J., Darby, S. E., Teruggi, L., Rinaldi, M., & Ostuni, D. (2015). A self-limiting bank
 1132 erosion mechanism? Inferring temporal variations in bank form and skin drag from high
 1133 resolution topographic data. *Earth Surface Processes and Landforms*, 40(12), 1600–1615.
 1134 <https://doi.org/10.1002/esp.3739>
 1135 Lininger, K. B., & Wohl, E. (2019). Earth-Science Reviews Floodplain dynamics in North
 1136 American permafrost regions under a warming climate and implications for organic carbon
 1137 stocks : A review and synthesis. *Earth-Science Reviews*, 193(March), 24–44.
 1138 <https://doi.org/10.1016/j.earscirev.2019.02.024>

- Lininger, K. B., Wohl, E., & Rose, J. R. (2018). Geomorphic controls on floodplain soil organic carbon in the Yukon Flats, interior Alaska, from reach to river basin scales. *Water Resources Research*, 54(3), 1934–1951.
- Lininger, K. B., Wohl, E., Rose, J. R., & Leisz, S. J. (2019). Significant floodplain soil organic carbon storage along a large high-latitude river and its tributaries. *Geophysical Research Letters*, 46(4), 2121–2129.
- Mann, P. J., Eglinton, T. I., McIntyre, C. P., Zimov, N., Davydova, A., Vonk, J. E., et al. (2015). Utilization of ancient permafrost carbon in headwaters of Arctic fluvial networks. *Nature Communications*, 6, 1–7. <https://doi.org/10.1038/ncomms8856>
- Matsubara, Y., Howard, A. D., Burr, D. M., Williams, R. M. E., Dietrich, W. E., & Moore, J. M. (2015). River meandering on Earth and Mars: A comparative study of Aeolis Dorsa meanders, Mars and possible terrestrial analogs of the Usuktuk River, AK, and the Quinn River, NV. *Geomorphology*, 240, 102–120. <https://doi.org/10.1016/j.geomorph.2014.08.031>
- McClelland, J. W., Holmes, R. M., Peterson, B. J., Raymond, P. A., Striegl, R. G., Zhulidov, A. v., et al. (2016). Particulate organic carbon and nitrogen export from major Arctic rivers. *Global Biogeochemical Cycles*, 30(5), 629–643. <https://doi.org/10.1002/2015gb005351>
- Midgley, T. L., Fox, G. A., & Heeren, D. M. (2012). Evaluation of the bank stability and toe erosion model (BSTEM) for predicting lateral retreat on composite streambanks. *Geomorphology*, 145, 107–114. <https://doi.org/10.1016/j.geomorph.2011.12.044>
- Miles, M. (1976). An investigation on riverbanks and coastal erosion, Banks Island, District of Franklin (Report of, pp. 195–200).
- Milliman, J. D., & Farnsworth, K. L. (2013). *River discharge to the coastal ocean: a global synthesis*. Cambridge University Press.
- Moody, J. A. (2022). The effects of discharge and bank orientation on the annual riverbank erosion along Powder River in Montana, USA. *Geomorphology*, 403, 108134. <https://doi.org/10.1016/J.GEOMORPH.2022.108134>
- Naito, K., & Parker, G. (2019). Can Bankfull Discharge and Bankfull Channel Characteristics of an Alluvial Meandering River be Cospecified From a Flow Duration Curve? *Journal of Geophysical Research: Earth Surface*, 124(10), 2381–2401. <https://doi.org/10.1029/2018JF004971>
- Naito, K., & Parker, G. (2020). Adjustment of self-formed bankfull channel geometry of meandering rivers: modelling study. *Earth Surface Processes and Landforms*, 45(13), 3313–3322. <https://doi.org/10.1002/esp.4966>
- Nanson, G. C., & Hickin, E. J. (1986). A statistical analysis of bank erosion and channel migration in western Canada. *Geological Society of America Bulletin*, 97(4), 497–504.
- Nilsson, C., Polvi, L. E., & Lind, L. (2015). Extreme events in streams and rivers in arctic and subarctic regions in an uncertain future. *Freshwater Biology*, 60(12), 2535–2546. <https://doi.org/10.1111/fwb.12477>
- Obu, J., Westermann, S., Kääb, A., & Bartsch, A. (2018). Ground Temperature Map, 2000–2016, Northern Hemisphere Permafrost. PANGAEA. <https://doi.org/10.1594/PANGAEA.888600>
- Obu, J., Westermann, S., Bartsch, A., Berdnikov, N., Christiansen, H. H., Dashtseren, A., et al. (2019). Northern Hemisphere permafrost map based on TTOP modelling for 2000–2016 at 1 km 2 scale. *Earth-Science Reviews*, 193(October 2018), 299–316. <https://doi.org/10.1016/j.earscirev.2019.04.023>
- Partheniades, E. (1965). Erosion and deposition of cohesive soils. *Journal of the Hydraulics Division*, 91(1), 105–139.

- Pastick, N. J., Jorgenson, M. T., Wylie, B. K., Minsley, B. J., Ji, L., Walvoord, M. A., et al. (2013). Extending Airborne Electromagnetic Surveys for Regional Active Layer and Permafrost Mapping with Remote Sensing and Ancillary Data, Yukon Flats Ecoregion, Central Alaska, 199(April 2012), 184–199. <https://doi.org/10.1002/ppp.1775>
- Pastick, N. J., Jorgenson, M. T., Wylie, B. K., Rose, J. R., Rigge, M., & Walvoord, M. A. (2014). Spatial variability and landscape controls of near-surface permafrost within the Alaskan Yukon River Basin. *Journal of Geophysical Research: Biogeosciences*, 119(6), 1244–1265.
- Pastick, N. J., Jorgenson, M. T., Wylie, B. K., Nield, S. J., Johnson, K. D., & Finley, A. O. (2015). Remote Sensing of Environment Distribution of near-surface permafrost in Alaska: Estimates of present and future conditions. *Remote Sensing of Environment*, 168, 301–315. <https://doi.org/10.1016/j.rse.2015.07.019>
- Payne, C., Panda, S., & Prakash, A. (2018). Remote sensing of river erosion on the Colville river, North Slope Alaska. *Remote Sensing*, 10(3). <https://doi.org/10.3390/rs10030397>
- Perkins, S. J., Edlund, K., Esch-Mosher, D., Eads, D., Harvey, N., & Brumby, S. (2005). Genie Pro: Robust image classification using shape, texture, and spectral information. *Proceedings of SPIE*, 5806, 139–148.
- Peucker-Ehrenbrink, B. (2009). Land2Sea database of river drainage basin sizes, annual water discharges, and suspended sediment fluxes. *Geochemistry Geophysics Geosystems*, 10. <https://doi.org/10.1029/2008gc002356>
- Pizzuto, J. (2009). An empirical model of event scale cohesive bank profile evolution. *Earth Surface Processes and Landforms*, 34(April), 1234–1244. <https://doi.org/10.1002/esp>
- Prowse, T. D., & Beltaos, S. (2002). Climatic control of river-ice hydrology: a review. *Hydrological Processes*, 16(4), 805–822. Retrieved from <http://dx.doi.org/10.1002/hyp.369>
- Prowse, T. D., & Culp, J. M. (2003). Ice breakup: A neglected factor in river ecology. *Canadian Journal of Civil Engineering*, 30(1), 128–144. <https://doi.org/10.1139/102-040>
- Rachold, V., Eicken, H., Gordeev, V. v., Grigoriev, M. N., Hubberten, H. W., Lisitzin, A. P., et al. (2004). Modern Terrigenous Organic Carbon Input to the Arctic Ocean. In R. Stein & R. W. Macdonald (Eds.), *The Organic Carbon Cycle in the Arctic Ocean* (1st ed., p. 378). Berlin, Heidelberg: Springer-Verlag. <https://doi.org/10.1007/978-3-642-18912-8>
- Randriamazaoro, R., Dupeyrat, L., Costard, F., & Gailhardis, E. C. (2007). Fluvial thermal erosion: heat balance integral method. *Earth Surface Processes and Landforms*, 32(12), 1828–1840.
- Raynolds, M. K., Walker, D. A., Balser, A., Bay, C., Campbell, M., Cherosov, M. M., et al. (2019). A raster version of the Circumpolar Arctic Vegetation Map (CAVM). *Remote Sensing of Environment*, 232(July). <https://doi.org/10.1016/j.rse.2019.111297>
- Rinaldi, M., & Casagli, N. (1999). Stability of streambanks formed in partially saturated soils and effects of negative pore water pressures: The Sieve River (Italy). *Geomorphology*, 26(4), 253–277. [https://doi.org/10.1016/S0169-555X\(98\)00069-5](https://doi.org/10.1016/S0169-555X(98)00069-5)
- Rinaldi, M., & Darby, S. E. (2007). Modelling river-bank-erosion processes and mass failure mechanisms: progress towards fully coupled simulations. In *Developments in Earth Surface Processes* (Vol. 11, pp. 213–239). Elsevier. [https://doi.org/10.1016/S0928-2025\(07\)11126-3](https://doi.org/10.1016/S0928-2025(07)11126-3)
- Rinaldi, M., & Darby, S. E. (2008). Modelling river-bank-erosion processes and mass failure mechanisms: progress towards fully coupled simulations. In H. Habersack, H. Piegay, & M.

- Rinaldi (Eds.), *Gravel-Bed Rivers VI: From Process Understanding to River Restoration* (Vol. 11, pp. 213–239). Elsevier.
- Rinaldi, M., Mengoni, B., Luppi, L., Darby, S. E., & Mosselman, E. (2008). Numerical simulation of hydrodynamics and bank erosion in a river bend. *Water Resources Research*, 44(9), 1–17. <https://doi.org/10.1029/2008WR007008>
- Rowland, J. C., Crosby, B., Schwenk, J., Piliouras, A., & Douglas, M. (2023). *Riverbank temperatures on the Selawik River, Alaska 2010-2012, and Koyukuk River, Alaska June to July 2018. Incorporating the Hydrological Controls on Carbon Cycling in Floodplain Ecosystems into Earth System Models (ESMs), ESS-DIVE repository*. ESS-DIVE (<http://ess-dive.lbl.gov/>). <https://doi.org/https://data.ess-dive.lbl.gov/datasets/doi:10.15485/1922885>
- Rowland, J. C., & Schwenk, J. (2019). *Global meta-analysis of published river bank erosion and migration rates*. ESS-DIVE (<http://ess-dive.lbl.gov/>). <https://doi.org/10.15485/1571181>
- Rowland, J. C., & Stauffer, S. (2019a). *Classified channel masks of portions of 13 rivers across the Arctic and areas of floodplain erosion and accretion ranging from 1973 to 2016*. ESS-DIVE (<http://ess-dive.lbl.gov/>).
- Rowland, J. C., & Stauffer, S. (2019b). *Pan-arctic river bank erosion and accretion, and planform metrics measured over intervals ranging from 1973 to 2016*. ESS-DIVE (<http://ess-dive.lbl.gov/>). <https://doi.org/10.15485/1571527>
- Rowland, J. C., Shelef, E., Pope, P. A., Muss, J., Gangodagamage, C., Brumby, S. P., & Wilson, C. J. (2016). A morphology independent methodology for quantifying planview river change and characteristics from remotely sensed imagery. *Remote Sensing of Environment*, 184. <https://doi.org/10.1016/j.rse.2016.07.005>
- Schuur, E. A. G., McGuire, A. D., Schädel, C., Grosse, G., Harden, J. W., Hayes, D. J., et al. (2015). Climate change and the permafrost carbon feedback. *Nature* 2015 520:7546, 520(7546), 171–179. <https://doi.org/10.1038/nature14338>
- Schwenk, J., Khandelwal, A., Fratkin, M., Kumar, V., & Foufoula-Georgiou, E. (2017). High spatiotemporal resolution of river planform dynamics from Landsat: The RivMAP toolbox and results from the Ucayali River. *Earth and Space Science*, 4(2), 46–75. <https://doi.org/10.1002/2016ea000196>
- Schwenk, J., Zussman, T., Stachelek, J., & Rowland, J. C. (2022). Rabpro: Global Watershed Boundaries, River Elevation Profiles, and Catchment Statistics. *Journal of Open Source Software*, 7(73), 4237. <https://doi.org/10.21105/joss.04237>
- Schwenk, J., Piliouras, A., & Rowland, J. C. (2023). *Observations and Machine-Learned Models of Near-Surface Permafrost along the Koyukuk River, Alaska, USA. Incorporating the Hydrological Controls on Carbon Cycling in Floodplain Ecosystems into Earth System Models (ESMs), ESS-DIVE repository*. ESS-DIVE (<http://ess-dive.lbl.gov/>). <https://doi.org/https://data.ess-dive.lbl.gov/datasets/doi:10.15485/1922517>
- Scott, K. M. (1978). *Effects of permafrost on stream channel behavior in Arctic Alaska: USGS Professional Paper 1068*. US Govt. Print. Off.
- Scrimgeour, G. J., Prowse, T. D., Culp, J. M., & Chambers, P. A. (1994). Ecological effects of river ice break-up: a review and perspective. *Freshwater Biology*, 32, 261–275.
- Shur, Y., Vasiliev, A., Kanevsky, M., Maximov, V., & Zaikanov, V. (2002). Shore Erosion in Russian Arctic. *Cold Regions Engineering: Cold Regions Impacts on Transportation and Infrastructure*, 736–747.
- Shur, Y., Jones, B. M., Kanevskiy, M., Jorgenson, T., Jones, M. K. W., Fortier, D., et al. (2021). Fluvio-thermal erosion and thermal denudation in the yedoma region of northern Alaska:

- Revisiting the Ikillik River exposure. *Permafrost and Periglacial Processes*, 32(2), 277–298. <https://doi.org/10.1002/ppp.2105>
- Simon, A., & Collison, A. J. C. (2002). Quantifying the mechanical and hydrologic effects of riparian vegetation on streambank stability. *Earth Surface Processes and Landforms*, 27(5), 527–546. <https://doi.org/10.1002/ESP.325>
- Stettner, S., Beamish, A. L., Bartsch, A., Heim, B., Grosse, G., Roth, A., & Lantuit, H. (2018). Monitoring inter- and intra-seasonal dynamics of rapidly degrading ice-rich permafrost riverbanks in the Lena Delta with TerraSAR-X time series. *Remote Sensing*, 10(1). <https://doi.org/10.3390/rs10010051>
- Striegl, R. G., Dornblaser, M. M., Aiken, G. R., Wickland, K. P., & Raymond, P. A. (2007). Carbon export and cycling by the Yukon, Tanana, and Porcupine rivers, Alaska, 2001–2005. *Water Resources Research*, 43(2), 2001–2005. <https://doi.org/10.1029/2006WR005201>
- Tananaev, N. (2016). Hydrological and sedimentary controls over fluvial thermal erosion, the Lena River, central Yakutia. *Geomorphology*, 253, 524–533. <https://doi.org/10.1016/j.geomorph.2015.11.009>
- Tananaev, N., & Lotsari, E. (2022). Defrosting northern catchments: Fluvial effects of permafrost degradation. *Earth-Science Reviews*, 228(June 2021), 103996. <https://doi.org/10.1016/j.earscirev.2022.103996>
- Tank, S. E., Raymond, P. A., Striegl, R. G., McClelland, J. W., Holmes, R. M., Fiske, G. J., & Peterson, B. J. (2012). A land-to-ocean perspective on the magnitude, source and implication of DIC flux from major Arctic rivers to the Arctic Ocean. *Global Biogeochemical Cycles*, 26(4). <https://doi.org/10.1029/2011GB004192>
- Terhaar, J., Orr, J. C., Ethé, C., Regnier, P., & Bopp, L. (2019). Simulated Arctic Ocean Response to Doubling of Riverine Carbon and Nutrient Delivery. *Global Biogeochemical Cycles*, 33(8), 1048–1070. <https://doi.org/10.1029/2019GB006200>
- Torres, M. A., Limaye, A. B., Ganti, V., Lamb, M. P., Joshua West, A., & Fischer, W. W. (2017). Model predictions of long-lived storage of organic carbon in river deposits. *Earth Surface Dynamics*, 5(4), 711–730. <https://doi.org/10.5194/esurf-5-711-2017>
- Tsyтович, N. A. (1975). *Mechanics of frozen ground*. (G. K. Swinzow, Ed.). Scripta Book Co., McGraw-Hill.
- University of Alaska Fairbanks Institute of Northern Engineering, District, U. S. A. C. of E. A., & Laboratory, U. S. A. C. of E. C. R. R. and E. (2019). *Statewide Threat Assessment: Identification of Threats from Erosion, Flooding, and Thawing Permafrost in Remote Alaska Communities*.
- U.S. Army Corps of Engineers. (2007). *Alaska Baseline Erosion Assessment: Erosion Information Paper - Huslia, Alaska*.
- Walker, H. J., & Arnborg, L. (1963). Permafrost and ice-wedge effect on riverbank erosion. In *Proceedings of the First International Conference on Permafrost* (pp. 164–171).
- Walker, H. J., Arnborg, L., & Peippo, J. (1987). Riverbank Erosion in the Colville Delta, Alaska. *Geografiska Annaler. Series A, Physical Geography*, 69(1), 61–70. Retrieved from <http://www.jstor.org/stable/521367>
- Wickert, A. D., Martin, J. M., Tal, M., Kim, W., Sheets, B., & Paola, C. (2013). River channel lateral mobility: metrics, time scales, and controls. *Journal of Geophysical Research-Earth Surface*, 118(2), 396–412. <https://doi.org/10.1029/2012jf002386>
- van de Wiel, M. J. (2003). *Numerical modelling of channel adjustment in alluvial meandering rivers with riparian vegetation*.

- Wild, B., Andersson, A., Bröder, L., Vonk, J., Hugelius, G., McClelland, J. W., et al. (2019). Rivers across the Siberian Arctic unearth the patterns of carbon release from thawing permafrost. *Proceedings of the National Academy of Sciences of the United States of America*, 1–6. <https://doi.org/10.1073/pnas.1811797116>
- Williams, J. R. (1952a). Effect of Wind-generated Waves on Migration of the Yukon River in the Yukon Flats, Alaska. *Science*, 115(2293), 519–520. <https://doi.org/10.1126/science.115.2993.519>
- Williams, J. R. (1952b). Effect of Wind-generated Waves on Migration of the Yukon River in the Yukon Flats, Alaska. *Science*, 115(2993), 519–520. Retrieved from <http://www.sciencemag.org>
- Williams, J. R. (1955). Observations of freeze-up and break-up of the Yukon River at Beaver, Alaska. *Journal of Glaciology*, 2, 488–495.
- Williams, P. J., & Smith, M. W. (1991). *The frozen earth*.
- Wohl, E., & Scamardo, J. E. (2022). Aufeis as a Major Forcing Mechanism for Channel Avulsion and Implications of Warming Climate. *Geophysical Research Letters*, 49(20), e2022GL100246. <https://doi.org/10.1029/2022GL100246>
- Woo, M. K. (1990). Consequences of climatic change for hydrology in permafrost zones. *Journal of Cold Regions Engineering*, 4(1), 15–20.
- Woo, M. K., & Winter, T. C. (1993). The role of permafrost and seasonal frost in the hydrology of northern wetlands in North America. *Journal of Hydrology*, 141(1–4), 5–31. [https://doi.org/10.1016/0022-1694\(93\)90043-9](https://doi.org/10.1016/0022-1694(93)90043-9)
- Woo, M. K., Kane, D. L., Carey, S. K., & Yang, D. (2008). Progress in permafrost hydrology in the new millennium. *Permafrost and Periglacial Processes*, 19(2), 237–254. Retrieved from <http://dx.doi.org/10.1002/ppp.613>
- Yang, D., & Peterson, A. (2017). River water temperature in relation to local air temperature in the Mackenzie and Yukon basins. *Arctic*, 70(1), 47–58. <https://doi.org/10.14430/arctic4627>
- Young, B., Yarie, J., Verbyla, D., Huettmann, F., Herrick, K., & Chapin, F. S. (2017). Modeling and mapping forest diversity in the boreal forest of interior Alaska. *Landscape Ecology*, 32(2), 397–413. <https://doi.org/10.1007/s10980-016-0450-2>
- Zar, J. H. (1999). *Biostatistical analysis* (4th ed.). New Jersey: Prentice-Hall, Inc.
- Zhang, T., Li, D., East, A. E., Walling, D. E., Lane, S., Overeem, I., et al. (2022). Warming-driven erosion and sediment transport in cold regions. *Nature Reviews Earth & Environment* 2022, 1–20. <https://doi.org/10.1038/s43017-022-00362-0>
- Zhao, K., Coco, G., Gong, Z., Darby, S. E., Lanzoni, S., Xu, F., et al. (2022). A review on bank retreat: Mechanisms, observations, and modelling. *Reviews of Geophysics*, 1–51. <https://doi.org/10.1029/2021rg000761>